# List of Major Changes

**Global changes:**

- Revision of text structure according to readability and story line
- Supplementary Material: Some Figures are put to a supplementary document
- We added an appendix section and moved some information into it

**Specific changes:**

- We rearranged Section 2 for a better story line and readability
- We adjusted some Figures according to the comments of the reviewer
- We reduced the number of acronyms to reduce confusion

# Point-by-point response to Reviewer #1

Florian Ehmele on behalf of the co-author

December 19, 2018

Thank you very much for your work and the useful and valuable comments that helped to improve the scientific quality of our manuscript. Please find below our reply to the individual points.

The authors have made great efforts in improving the manuscript. The paper structure looks better, and it appears to be a complete model development study after adding a comparison with another model.

We thank you for your positive feedback.

But I think the description of the model algorithm should be simplified, especially from those previous studies. But the sections developed by the authors should be highlighted. In this way, the readability will be improved and the novelty will be highlighted.

We agree, that a rearrangement and tightening of the model description section would be helpful especially as the comments of the other reviewer go into the same direction. We have fixed this in the revised version of the manuscript by shortening the description of the original linear model and rearrange Section 2: General Description, Description of the original approach, modifications made by us and a Section on pre-preparations and general simulation procedure (flowchart).

Another aspect is not so clear. The procedures for extreme events do not include a component for time series generation. For weather generator, it usually generates time series of wet events. However, it appears that the current procedure develop the PDFs of different seasons based on a group of extreme wet events, and then used to generate another group of extreme events. If so, how to apply the results for future risk assessment?

You are right, based a seasonal PDFs of historic extreme events, a stochastic event set is computed with a certain number of at first independent events. It is possible to estimate a corresponding somehow continuous time period as it is described in Section 6: Counting the number of events in the stochastic event set exceeding a defined threshold, for example, in our case the $99^{th}$ percentile of the observations (regarding spatial mean precipitation) and normalize it with its probability. The resulting total time span $T_{SPM}$ can be used to estimate the return period of every single event (like in Figure 15), to rank the events, and to estimate a new PDF (Gumbel) which can be used for the risk assessment. The rainfall events can be used as input for hydrological rainfall-runoff-models. We have added a statement in the conclusions on how to transfer the results to future risk assessments.

# Point-by-point response to Reviewer #4

Florian Ehmele on behalf of the co-author

December 19, 2018

Thank you very much for your work and the useful and valuable comments that helped to improve the scientific quality of our manuscript. Please find below our reply to the individual points.

Dear Florian Ehmele and Michael Kunz,
I have now finished reading your manuscript entitled “Flood-Related Extreme Precipitation in Southwestern Germany: Development of a Two-Dimensional Stochastic Precipitation Model”. I found the manuscript interesting and I think the hydrological community will benefit from the advancements in Smith and Barstad’s stochastic rainfall model you are suggesting. The manuscript fall within the topics cover in HESS, and I believe that after revising the text the paper can be accepted for publication.

Thank your very much again for you positive feedback on the general topic of the paper.

Saying that, I have struggled to read the paper till the end. In its present form the text is hard to read and to follow. My main comments are therefore related to the structure and length of the text:

- The text is too long. I suggest moving some of the Tables and Figures to the supplementary material (SI) – see some suggestions in the specific comments below. The same goes to the text itself – some of the descriptions can be summarized in a Table (list of model parameters, for example) and some can be moved to the SI. In addition, the text can be shorten in many places. For example, Section 3 (data sets) could be summarized in a single page (2.5 pages currently). The first sub-section describing the rainfall product can be summarized in two sentences, refereeing to REGNIE and indicating the product limitations.

After rereading the paper again, we agree that at many places the text can be tightened. Saying that we tried to rephrase the text without loosing to much necessary information. We follow the suggestion to move some of the Figures to a supplementary document, and we moved some information to an appendix.

- There are many replicas in the text that need to be eliminated. For example, Section 2.6 “Stochastic modeling of precipitation events with SPM2D requires the adjustment of appropriate probability density functions (pdfs) to all input parameters…” and in the beginning of Section 5.1 “Stochastic model simulations are based on pdfs that are adjusted to the required parameter…”. The text should be concise as possible, especially when the text is of technical nature like in this manuscript.

We carefully checked the paper again for replicas and eliminated them as far as possible.

- Some restructuring is needed. In many cases I thought that information is missing and that the text is incomplete just to realize that the information I looked for is written later in the text. For example, in page 5 line 15 you mention that “R may become negative” and only later (page 6 line 25) you explain that even if it is negative you consider it to be zero. Another example, the model is briefly described at the introduction and then again in Section 2.1. I suggest to follow a simple structure: general introduction, description of the model component, model calibration (general calibration procedure, not tailored to the case study, so readers can understand what input is required and how to calibrate the model), short description of the study area, short description of the data sets, calibration and results of the case study, and conclusions.

We also agree in this point with the reviewer and tried to rearrange the text that information is given at the right place (see also specific comments below). We removed the mode description from the introduction to keep it general. As a restructuring of Section 2 was also recommended by the other reviewer we applied it as follows: General Description of the complete stochastic model (2.1), brief description of the underlying linear orographic model by Smith and Barstad with its components (2.2), description of the modifications implemented in this study (2.3), and pre-preparations and general simulation procedure (2.4). We now think that our modifications are more highlighted and the overall operating principles became more clear. At this point we need to clarify that the given calibration in Sect. 4 is the general procedure using the training sample of historic extreme events and the case study (4.4) is an example (out of that sample) of the model output after calibration.

Below please find my specific comments to the text. I hope that you will find my comments useful and take my criticism positively. I value your study and I hope they will assist in improving the manuscript.

Again many thank, your comments indeed have been very helpful.

Specific comments
[page line]

[2 1] Actually, IDF curves can be estimated over large areas using gridded information from remote sensing. In recent years there were several advances in this direction. Search, for example, for recent publications by Francesco Marra.
[2 4-6] For more recent studies were rainfall generators were used to compute spatially distributed IDF curves I can suggest the Authors to also consider two recent papers that we (Peleg et al., 2017 and 2018) have published that address this topic explicitly.
Peleg et al. (2017). Partitioning the impacts of spatial and climatological rainfall variability in urban drainage modeling. Hydrology and Earth System Sciences, 21(3), pp.1559-1572.
Peleg, N. et al. (2018). Spatial variability of extreme rainfall at radar subpixel scale. Journal of Hydrology, 556, pp.922-933.

Thanks for mentioning this new and interesting studies. We updated the introduction concerning this studies.

[2 14-25] This paragraph belongs to the method section, where the model is described.

Moved to and included in Section 2.1.

[4 3] Why only stratiform clouds? I see in eq. (1) that the convection component is also consider. I suspect that Eq 1 is not referring to the original model but to the developments you added later. Maybe first describe simply the original model as it, and then added a section explaining the changes you are suggesting.

The SPM2D is designed for widespread heavy precipitation related to pluvial flood events for which convection is of minor importance. Nevertheless convection can appear atop stratiform clouds influencing the very local precipitation distribution. This was the reason for us to implement this term. Equation 1 gives the total precipitation as it is calculated in the complete SPM2D and includes the original Smith-Barstad model as well as our modifications. As mentioned to the general comments, we rearranged Section 2 completely, so this should become clear.

[4 7] “large scale lifting”. What do you mean by that? upward lifting (i.e. omega component)? Isn't that part of vertical convection?

We rephrase the according text for clarification. Large-scale lifting is referred to the omega-equation with its components of vorticity advection, warm air advection and diabatic phase transition which lead to large-scale vertical motions. Conversely, convection (in meteorology) describes small-scale thermally driven circulations (e.g. buoyancy) which is a different type of physical process, and so we differentiate it accordingly.

[4 9] "rSPM". If I understand right, you are modifying the original SPM2D model to be a reduced complexity model for some components while adding additional components that were not part of the original model. The fact that you have two names for the same model (SPM2D and rSPM) is confusing. Mention the changes made to the model (can also be given in a form of a table – original model components and the new model components) so it will be clear what is what.

SPM2D is the new complete model, rSPM is meant as the original Smith-Barstad model. Along with the restructuring we changed the name to SBM to separate it more distinctly. We also reduced the number of acronyms (see further comments below).

[4 9] "we included two additional precipitation components". Which are not part of the original Smith and Barstad model? If this is the case, then equation 1 should be with only the components originally used in SPM2D and a new equation 2 is to be given with the components of rSPM. That will also resolve my above comment related to the stratiform cloud.

This should be clear now with the new text structure.

[4 11-13] The sentence is not that clear, please rephrase.

We fixed this.
[general comment] Please add a table that summarize the parameters of the model.

After tightening and rearranging the text, we think an additional table is not necessary, especially as Table 2 (Sect. 5.1) gives this overview when summarizing the results of the pdf estimation which is the required part to run the SPM2D in stochastic mode.

[4 15] "is simulated". Simulated how? For each year the total numbers of events and the length for each events are sampled from a given distribution? If so, which distribution is used? Please give more details here.

This should be clear now in the Sect. 2.4.2 giving a description of the general simulation procedure. A total number of independent events (here 10,000) is simulated using the estimated seasonal pdfs. Which type of pdf best fits the observed distribution for each variable is given later in the results part (i.e. Table 2, Sect. 5.1) and not of importance at this point. The stochastic event set than can reallocated to a certain time period as described in Section 6, which then is useful e.g. for risk assessments.

[4 18-19] I am missing some information here. What is the spatial and temporal resolution of the model? Is the model daily or sub-daily?

This should now be clarified within the introductory paragraph to Section 2 and Section 2.4.2. The spatial resolution of the model is 1 km² in accordance to the mainly used REGNIE observations. The temporal resolution of the SPM2D is 24 hours. Within every time step, the stochastic precipitation parts of fronts and convection are calculated once and treated as footprints in daily precipitation. The SBM parts of orographic and synoptic background precipitation are calculated twice in

accordance to the 12-houly soundings we used and to account for slightly variations of the ambient conditions during the day. We add this comment to the text.

[4 30] “sounding data”. Can also be estimated from other sources, such as reanalysis data? A matter for a latter discussion.

We use sounding data in this study, but yes, vertical profiles can be estimated from reanalysis data as well. We add a comment on that to the conclusions.

[Figure 2] What are all the larger/smaller values from zero refer to? For example, for Roro, which arrow is for values larger than zero and which arrow to follow when values are smaller than zero? Rtot will always be larger than zero as only wet events are consider, no?

We add two additional arrows for the cases of Roro < 0 and Rfront < 0 to Fig. 2. With the restructured text and the answers to previous comments, this should also be clear now. Both Roro and Rfront can attain negative values in descent regions due to evaporation. These negative values are taken into account in the summation of Rtot. And the end, values of Rtot <0 are truncated away as it is non-physical. Therefore, Rtot can reach zero at some grid points but regrading spatial means only wet events are simulated with SPM2D.

[5 9] I can understand why the time sacles are constant in time, but why they are constant in space?

This is an assumption of the original Smith-Barstad model and one reason why the extent of the model domain is limited. The time scales are assumed to be homogeneous regrading mesoscale areas. We add a comment on that in the text.

[5 15] And is consider negative when embedded in equation 1 or is set to zero?
[6 24-26] OK, that answer my previous question. This should have been mentioned earlier.

See above reply on the comment on Figure 2. Fixed in the text.

[7 4] I do not see it in equation 6. Did you meant eq. 7?
[7 11] Eq. 7. Equation 6 is still on the k,l plane.

We combined the former Equations (4) and (6) to a final function for orographic precipitation. The new Equation (4), then, visibly contains all the modifications made. With that, the text should be better understandable.

[7 15] “whereas Coro is constant over the whole domain”. From Fig. 3 it seems that Coro is changing along the x-y plane and is not constant over the whole domain. Is it constant in time? I guesses you meant here to say that Coro is affecting all grid cells in all times.

Coro is a constant number which affects all grid points and throughout all events which reduced the orographic part by a certain degree. In regions with high values of Roro the effect of Coro is more pronounced than in regions where Roro is of less importance. We modified the according text for better understanding.

[8 2-4] This explanation should be moved up, after equation 1 is introduced.

Fixed.

[8 30] The value of Cfront is determined from a distribution? Or is it constant for each season? Depend on the wind direction? Please add information on how the values of Cfront are defined.

As described in the text, a front is implemented as a rectangular area with infinitely extent along the front-parallel axis and a Guassian-shaped smoothing along the front-normal axis (we also adjusted the notations in Figure 4). The each time step, the maximum of this distribution is given by Cfront using the corresponding seasonal differentiated pdfs and than smoothed to the borders of the rectangular. We modified the text for better understanding. Furthermore, Cfront is independent from wind direction.

[9 10] “Note, however, that the model is not foreseen to simulate purely convection”. But, often the most extreme rainfall is (almost) purely convective in nature - isn't that contradict the purpose of this study, to explicitly account for the extreme (200-y return period) rainfall events?

You have to separate between pluvial flood events and flash floods. Flash floods are driven by almost purely (free) convective precipitation. Pluvial floods along the major rivers, which are the focus of this study, are not related to free convection but are caused by widespread long-lasting precipitation from stratiform clouds where convective cells can be include leading to locally enhanced rainfall totals. This is the reason why we add a convective precipitation part Rconv, but it is different from (free) deep moist convection. We modified the text for better understanding.

[10 9] “convective cells”. It makes sense to follow the cell structure only if the temporal resolution of the model is hourly or sub-hourly (is it? reading so far I couldn't find the information about the temporal resolution of the model), with coarser resolution you cannot detect cells' structure anymore.

As mentioned above the SPM2D is not foreseen to simulate purely convection in detail. The expression “convective cell” might be inappropriate in this case, so we changed it to “footprint” which is more of what was the intention – regions of enhanced precipitation due to convection visible in daily totals.

[10 12] I get from this that the grid cell size is 1 km? That information should be written somewhere.

We add a short paragraph on that at the beginning of Section 2.

[11 3] “the spatial distribution of Cconv randomly varies between the given limits”. Why? Anyhow you do not try to capture the spatial structure of the cells, so why adding another level of complexity?

Even though convection is simplified and seen as footprints in daily precipitation, it is adequate to vary Cconv in between such a footprint instead of assigning a constant value for the entire footprint area. In an extreme case a footprint can be of 300km length and in order of several 10km width. Assigning a constant value to this large area would produce a less realistic precipitation distribution, so we vary Cconv and smooth it at the end. Nevertheless, for potential subsequent hydrological simulations widespread precipitation is of greater importance and the difference between a fixed or a varying Cconv is negligible. We add a comment to the text.

[12 2] March-April-May, MAM from hereon. Same for the other seasons.

Fixed.

[Table 1] Instead of list of distributions that were examined, I suggest having a table summarizing the distribution used for each of the variables.
- Further reading, I see that this information is given in Table 3. I thus do not see the need in having Table 1 (maybe as supplementary material) and suggest to remove it.

We agree and put Table 1 into an appendix section as it is useful for the pdf acronyms.

[16 6] r refer here to the spatial correlation of a given rain field?

Despite putting the description of the skill score to the appendix section, we changed the text to clarify this comment. r in this case is the Spearman correlation coefficient between the observed and simulated precipitation field (2D).

[Figure 7] Can be moved to the supplementary material.
[Figure 9] can be moved to the SI as well.

As recommended we put both figures into a supplementary document.

[21 7-11] There is more than the mean areal rainfall that needs to be consider when comparing maps of extreme rainfall. For example, how well the structure (dimension and location) of the heavy rainfall (e.g. above 50 mm per day) are reproduced?

Such information, actually, is given at the beginning of the case study when describing the spatial distribution of the observed and simulated precipitation filed. To pronounce it a little bit more we add hard numbers of overall maximum precipitation and the area exceeding R=50mm.

[26 7] Simulated how? I guess that for a given event the parameters were sampled from the relevant distributions independently. Are the model variables (e.g. the lapse rates) corss-correlated and, if so, is the cross-correlation accounted for in the model (for example, by sampling the parameters from the pdfs using copulas). Please provide more information here.

The simulation procedure is given in Sect. 2.4.2. but we also add some information at this point: Every single event of the 10,000 has a specific duration leading to a total number of approx 31,500 days. For each of the input variables a vector of values of the same length (31,500) is estimated using the corresponding pdfs giving the required input for each day. The variables are treated as independent. A correlation analysis was given in Sect. 5.1 and reveals less correlations so that a coupling of pdfs via copulas is not necessary.

[new table] I suggest adding a new table summarizing the different models and experiments (rSPM10k, CCLM, rSPM...). It becomes difficult to follow all the names.

During the revisions we conclude that some of the acronyms are not necessary or not any more. Therefore, we reduced the number of names to a minimum so that an extra table is not required.

[Figure 16] SI

Done.

# Flood-Related Extreme Precipitation in Southwestern Germany: Development of a Two-Dimensional Stochastic Precipitation Model

Florian Ehmele[1] and Michael Kunz[1,2]

[1]Institute of Meteorology and Climate Research, Karlsruhe Institute of Technology (KIT), Hermann-von-Helmholtz-Platz 1, 76344 Eggenstein-Leopoldshafen, Germany.
[2]Center for Disaster Management and Risk Reduction Technology (CEDIM), KIT - Karlsruhe, Germany

*Correspondence to:* Florian Ehmele (florian.ehmele@kit.edu)

**Abstract.** Various ~~application fields~~ fields of application, such as ~~insurance industry risk assessments for the~~ risk assessments of the insurance industry or the design of flood protection systems, require reliable precipitation statistics in high spatial resolution, including estimates for events with high return periods. Observations from point stations, however, lack of spatial representativeness, especially over complex terrain. ~~Thus, they do not reliably represent the heavy tail of the distribution function. Common~~ Current numerical weather models are not capable of running simulations over thousands of years. This paper presents a new ~~numerical method to simulate larger-scale precipitation fields stochastically,~~ method for the stochastic simulation of widespread precipitation based on a linear theory describing orographic precipitation and additional functions that consider synoptically driven rainfall and embedded convection in a simplified way. The model is initialized by various statistical distribution functions describing prevailing atmospheric conditions ~~,~~ such as wind vector, moisture content, or stability, estimated from radiosonde observations for a limited sample of ~~the 200 strongest rainfall eventsobserved.~~ observed heavy rainfall events. The model is applied for the stochastic simulation of heavy rainfall over the complex terrain of Southwest Germany. It is shown that the model ~~, despite its simplicity, yields~~ provides reliable precipitation fields ~~. Differences~~ despite its simplicity. The differences between observed and simulated rainfall statistics are small, being in the order of only $\pm$ 10 % for return periods of up to 1,000 years.

## 1 Introduction

~~Persistent precipitation~~ Severe pluvial flood events resulting from persistent rainfall over large areas ~~and the resulting widespread flooding frequently cause major damage in Central Europe in the order~~ has the potential to cause high economic losses of several billion ~~Euro~~ euros (EUR) ~~per event~~in central Europe. In Germany, the two extreme floods ~~in~~ of 2002 and 2013 with estimated return periods of more than 200 years (Schröter et al., 2015) ~~collectively caused~~ resulted in losses of more than EUR 22 billion ~~in economic losses~~ (inflation adjusted to 2017; MunichRe, 2017). ~~Beside these~~ In addition to these rare extreme events, ~~smaller floods with higher frequencies~~less severe floods with shorter return periods, such as ~~those~~ in 2005, 2006, 2010, and 2011 (Uhlemann et al., 2010; Kienzler et al., 2015), also contribute significantly to the large ~~damage potential associated with floods .~~

average annual losses from floods of EUR 1.1 billion in Germany in the last 30 years (MunichRe, 2017). Flood risk estimation, for example, for insurance purposes or for the design of appropriate flood ~~mitigation~~ protection systems, requires ~~the dependable statistical analysis of extreme~~ comprehensive statistical analyses of both runoff and rainfall. Traditionally, ~~these extremes~~ extremes associated with the latter have been estimated at point stations from intensity-duration-frequency (IDF) with extreme value statistics being applied (Koutsoyiannis et al., 1998). This method, however, implies two ~~drawbacks~~major difficulties: (i) the low ~~spatial representativeness~~ density of point observations and their limited representativeness in particular over complex terrain, and (ii) the limited observation period ~~so~~ with the consequence that not all possible extreme configurations enter the samples.

To account for the former ~~shortcoming, either~~ issue, geostatistical interpolation routines, such as kriging (Goovaerts, 2000), or techniques ~~that relate precipitation to both orographic characteristics and atmospheric parameters (e.g., Basist et al., 1994; Drogue et al., 2002) are used. Shortcomings resulting from these methods are the lack of representativeness of station data with respect to the surroundings,~~ relating precipitation and ~~the neglect of dynamical and thermodynamical processes decisive for real precipitation events.~~ orographic or atmospheric characteristics (e.g., Basist et al., 1994; Drogue et al., 2002) have been applied. Recently, Marra et al. (2017) showed that IDFs can be reliably estimated from remote sensing data, such as weather radars, with high spatial coverage. However, the conversion from radar reflectivity to rain intensity leads to high uncertainty mainly because of the unknown drop size distribution in combination with the radar reflectivity being proportional to the drop diameter in the sixth power. Comparing IDFs obtained from radar data with point observations on a local scale, Peleg et al. (2018) found that the spatial IDFs tend to underestimate rainfall intensity for short return periods, and that the natural variability of extreme rainfall increases the uncertainties of the IDFs for longer return periods and larger areas.

To account for the limited observation period, several studies have employed stochastic weather generators to simulate precipitation events at single grid points (e. g., Richardson, 1981; Furrer and Katz, 2007; Neykov et al., 2014). A recent study by Cross et al. (2017), for example, introduced a censored rainfall modeling approach designed to reduce the underestimation of extremes. Albeit considering the long-term variability of precipitation, which leads to more reliable estimates for extremes, these approaches still lack spatial representativeness.

~~In the present study, we present a two-dimensional stochastic precipitation model (SPM2D) that allows for simulating a large number of precipitation fields using a high spatial resolution. Large sample sizes of several thousand events are required to obtain robust estimates of the hazard for high recurrence periods, like the one-in-200-year eventsthat have to be considered by insurance companies. Common numerical weather models are not capable of simulating thousands of years~~ Furthermore, robust estimates of precipitation extremes with high return periods, for example, for a one-in-200-year event, require a large sample size of several thousands of events. Current numerical weather prediction (NWP) models, though having a high spatial resolution of several kilometers, are not able to simulate thousands of events due to their complexity and the resulting ~~long computation time~~high computing costs.

~~The core of our~~ In this study we present a two-dimensional stochastic precipitation model (SPM2D~~is the diagnostic linear model approach for orographic precipitation according to Smith and Barstad (2004). The model considers wave dynamicsin~~

terms of the linearized equations of a stratified, non-hydrostatic flow over mountains (Smith, 1980). Input parameters are atmospheric flow quantities connected to precipitation, such as stability), which was designed for the stochastic simulation of a very large number of precipitation fields in high spatial resolution. Precipitation associated with different processes such as orographically-induced wave dynamics, moisture scaling height, precipitable water, or flow speed, all estimated large-scale lifting, or embedded convection is described by simplified parameterizations and combined linearly. Inclusion of several physically based tuning parameters of the model helps to keep track to precipitation patterns of real events. The model relies on several input parameters such as wind speed and direction, static stability, or moisture obtained from radiosoundings. Additional internal free parameters, such as characteristic time scales for cloud water conversion and fallout, serve as calibration parameters. The Smith and Barstad (2004) model has been successfully applied in various regions: e. g. several locations in the United States (Barstad and Smith, 2005), Iceland (Crochet et al., 2007), Southwest Germany (Kunz, 2011), or Southern and Northern Norway (Caroletti and Barstad, 2010; Barstad and Caroletti, 2013). Despite the fact that characteristic time scales and background precipitation may vary from one situation to another, it is found that simulations using fixed values for By doing so, the input parameters have to keep constant over the whole investigation area and for time period of the soundings, usually 12 hours. For the stochastic simulations, these input parameters are varied randomly based on appropriate probability density functions (pdfs) derived from a representative sample of historical heavy rainfall events. Because precipitation regimes in summer and winter vary significantly, we seasonally differentiate our analyses. The SPM2D is one component of a novel risk assessment method to quantify the probable maximum loss for a 200-year event (PML200) by considering simultaneous flooding along the main river networks. This paper, however, discusses only on the precipitation/hazard component.

The paper is structured as follows: Section 2 introduces the basic concept of the free parameters yield trustworthy results. In our approach, we added two additional components to the orographic and background precipitation: synoptic-scale fronts and convection embedded into mainly stratiform clouds (Fuhrer and Schär, 2005). Whereas the former component may enhance (or reduce in case of absence) precipitation over larger areas, the latter may lead to locally slightly enhanced totals. SPM2D. Section 3 briefly describes the data sets used in this study. Section 4 presents the results of the calibration based on a set of 200 representative historical heavy rainfall events and examines sensitivities of the model depending on varying ambient conditions. Section 5 shows some characteristics of the selected events. Results of the stochastic simulations are discussed in Section 6, and Section 7 lists some conclusions. Further information are given in a short appendix and supplementary material.

In the present study, we applied the

## 2 Stochastic Precipitation Model

The SPM2D to both single historical events with heavy rainfall (training events ) and over a long-term period of several thousand years (validation events). In the latter case, the required model parameters are estimated from probability density functions (pdfs) and are stochastically selected. In this application, we fixed the internal free parameters to constant values

~~estimated by thorough calibration. Because precipitation regimes in summer and winter vary significantly, we seasonally differentiate our analyses.~~

model is designed for the simulation of widespread, pluvial precipitation over complex terrain such as low mountain ranges, a typical feature of European topography. The investigation area for this study is the Federal State of Baden-Württemberg (BW) in Southwest Germany ~~, which extends from 46.6 to 50.8° N and from 6.9 to 11.1° E~~ (Fig. 1). The terrain exhibits a certain degree of complexity ~~:~~ with the broad Rhine Valley with elevations of 100–200 m bounded by the Vosges Mountains (France) to the west and the Black Forest mountains to the east~~;~~. The highest peak is the Feldberg with a maximum elevation of 1493 m ~~(Feldberg) in Southern Black Forest; and~~ in southern Black Forest. To the northeast, the topography is more flat with some rolling terrain~~to the northeast~~. Annual precipitation ~~is~~ varies between 600 mm (southern Rhine Valley) and approximately 2000 mm (southern Black Forest).

~~The presented SPM2D is one component of a risk assessment methodology that estimates the risk for a local direct insurer by quantifying the maximum probable loss for a 200-year return period (PML200). The other risk assessment components, however, are not further discussed in this paper.~~

~~The paper is structured as follows: Section 2 introduces the basics of the SPM2D. Section 3 briefly describes the data sets used in this study. Section 4 presents the results of the calibration based on a set of 200 historical heavy rainfall events and gives a sensitivity study of the model depending on varying ambient conditions.Section 5 shows some characteristics of the selected events. Results of the stochastic simulations are discussed in Section 6, and Section 7 lists some conclusions.~~

## 3 ~~Stochastic Precipitation Model~~

As described in the following Sect. 2.2, orographic precipitation is computed in Fourier space, and therefore, the model domain has to be symmetric with $2^n$ ($n$ is a positive integer). In this study we used a 512×512 grid with a resolution of 1 km$^2$. Also note that the assumption of horizontal homogeneous conditions, which is a prerequisite for the orographic model, limit the overall size of the model domain.

After a description of the model components (Sect. 2.1 – 2.3), some necessary preparations and an overview of the general simulation procedure are presented in Sect. 2.4.

### 2.1 General description

~~The SPM2D, designed for widespread precipitation from essentially stratiform clouds,~~ Overall, the model SPM2D quantifies total precipitation $R_{\mathrm{tot}}$ from the linear superposition of four ~~processes and terms~~terms, each of them representing a specific precipitation process:

$$R_{\mathrm{tot}} = R_{\mathrm{oro}} + R_{\infty} + R_{\mathrm{front}} + R_{\mathrm{conv}}\,. \tag{1}$$

The first two components of Eq. (1) originate from the diagnostic linear model of orographic precipitation according to Smith and Barstad (2004) and Barstad and Smith (2005), hereafter referred to as Smith-Barstad-Model (SBM). The first

component, $R_{oro}$ ~~estimates orographic rain enhancement, representing the central core of the SPM2D for complex terrain , as for instance those in BW.~~, quantifies rain enhancement as a consequence of orographically induced lifting. Over complex terrain and for high amounts of incoming water vapor flux (Kunz, 2011), this part dominates the other three in (Eq. 1). The next term, $R_{\infty,}$ is the background precipitation related to synoptic-scale lifting. According to the $\omega$-equation, large-scale lifting~~. These two parts originate from the linear orographic precipitation model of Smith and Barstad (2004) and Barstad and Smith (2005) with a few modifications, hereinafter referred to as reduced SPM2D (rSPM). In an extension of the rSPM, we included two additional~~

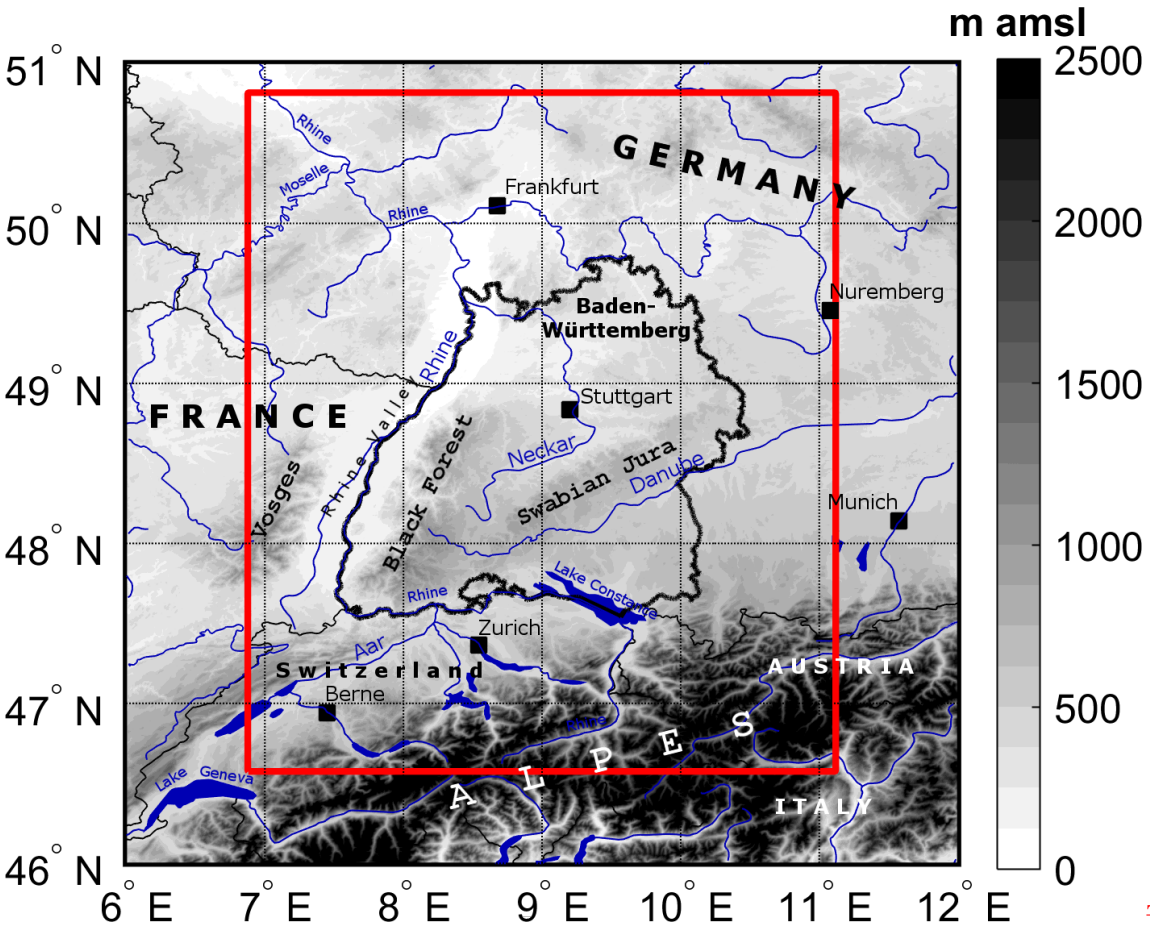


~~Topographic map of Southwestern Germany and surrounding areas with main river networks and lakes as well as substantial orographic structures; The national borders (slim solid black contours) and the border of the Federal State of Baden-Württemberg (bold solid black contour) are shown as well as the model domain (red box).~~

**Figure 1.** Topographic map of Southwestern Germany and surrounding areas with main river networks and lakes as well as substantial orographic structures. The national borders (slim solid black contours) and the border of the Federal State of Baden-Württemberg (bold solid black contour) are shown as well as the model domain (red box), which extends from 46.6 to 50.8° N and from 6.9 to 11.1° E.

precipitation , preferably occurring downstream of troughs (low pressure systems at higher levels), is the result of three different mechanisms: positive vorticity advection increasing with height (or vice versa); maximum of diabatic phase transitions; and maximum of warm air advection. Even though lifting results from the superposition of these three mechanisms, we do not split $R_\infty$ accordingly, as the single forcing terms cannot be estimated from vertical soundings used as input data in our approach (see Section 3.2).

As the SBM does not reliably reproduce the observed spatial variability of precipitation also over flat terrain for physical reasons (Kunz, 2011), we have implemented two additional components: $R_{\mathrm{front}}$ to account for precipitation related to synoptic consider precipitation associated with synoptic-scale fronts, and $R_{\mathrm{conv}}$ to consider related to embedded convection atop mainly stratiform clouds (e.g., Fuhrer and Schär, 2005; Kirshbaum and Smith, 2008). These two components were included because the related processes significantly contribute to the total precipitation amount and linear theory, at the same time, tends to an underestimation of low intensities (e.g., Kunz, 2011).

The SPM2D is an event-based model. Instead of simulating continuous long-term periods of several years, a specific number $n_{\mathrm{E}}$ of independent events with various duration $t_{\mathrm{ev}}$ occurring during different seasons is simulated. The individual components are discussed more detailed in the following Sections. Starting the iteration loop over $n_{\mathrm{E}}$ events, first, the characteristics season and duration $t_{\mathrm{ev}}$ are allocated to the event (Fig. 6). Next step is the computation of the precipitation fields within the loop over $t_{\mathrm{ev}}$. The components of the total precipitation in Eq. (1) are separated into two types: of stratiform clouds on a local scale (e.g., Fuhrer and Schär, 2005; Kirshbaum and Smith, 2008). While the former component can modify the entire precipitation field, the latter can lead to enhanced totals on the local scale. Deep moist convection, however, is not considered as it is not relevant for larger river floods. Note that both $R_{\mathrm{oro}}$ and $R_\infty$ are simulated 12-hourly (2 times a day), while $R_{\mathrm{front}}$ and $R_{\mathrm{conv}}$ are calculated 24-hourly (once a day). The linkage between the precipitation components and the corresponding input variables (pdfs; parameters) is also shown in Fig. 6. Note that the internal free model parameters are set to constant values for the entire simulation (illustrated as shaded box).After each 24-hour period, the total precipitation can attain negative values in descent areas. Negative values of total precipitation $R_{\mathrm{tot}}$ sums up according , however, are physically not meaningful and are therefore truncated away (i.e., $R_{\mathrm{tot}} = \max(R_{\mathrm{tot}}, 0)$ in Eq. (1). In case $t_{\mathrm{ev}}$ is reached, the computation goes on to the next event until $n_{\mathrm{E}}$ events have been simulated. Flow chart of the individual components within the SPM2D (solid boxes) and the corresponding input variables (pdfs; dashed boxes). Iteration loops are highlighted as ellipsis or bold dashed arrows. The constant model parameters are illustrated as shaded box.

Since the purpose of the model is to stochastically simulate a large number of several thousands events, the results can be used to robustly estimate rare events, such as the one-in-200-year events that the insurance industry must consider (probable maximum loss, PML200). The prerequisite, however, is a decent simulation of single events.

## 2.2 The Smith-Barstad Model (SBM)

## 2.3 Orographic precipitation

~~The linear precipitation model of Smith and Barstad (2004) and Barstad and Smith (2005), which is briefly described in this subsection, is~~ The linear orographic model SBM (Smith and Barstad, 2004; Barstad and Smith, 2005) is a simple yet efficient way to compute precipitation over complex terrain. ~~A total number of only seven atmospheric parameters estimated from sounding data (see Sect. 3.2) is required to run the model. It~~ It has been successfully applied in various regions around the world; e. g. several locations in the United States (Barstad and Smith, 2005), Iceland (Crochet et al., 2007), Southwest Germany (Kunz, 2011), or Southern and Northern Norway (Caroletti and Barstad, 2010; Barstad and Caroletti, 2013).

### 2.2.1 Orographic precipitation

The SBM is based on the linear theory of three-dimensional (3D) ~~linear flow according to Smith (1980) and Smith (1989). Thus, it~~ stratified, hydrostatic flow over mountains with uniform incoming horizontal wind speed and stability (Smith, 1980, 1989). It explicitly considers linear flow effects evolving over mountains, such as upstream-tilted gravity waves or flow that goes around rather than over an obstacle in the case of low wind speed, high static stability, and/or large mountains (i. e. small Froude numbers). It is assumed that saturated lifting produces condensed water that falls to the ground after a certain time shift (Jiang and Smith, 2003). Thus, precipitation on the ground is directly related to the condensation rate.

One of the key components of the linear model is a pair of linear steady-state equations for the advection of vertically integrated cloud water and hydrometeor density ~~, $q_c$ and $q_h$,~~ during characteristic time scales ~~:~~

$$\mathbf{v}\cdot\nabla q_c = S(x,y) - \frac{q_c}{\tau_c},$$

$$\mathbf{v}\cdot\nabla q_h = \frac{q_c}{\tau_c} - \frac{q_h}{\tau_f},$$

~~where $\tau_c$ and $\tau_f$ are time scales for~~ of cloud water conversion $\tau_c$ and the fallout of hydrometeors $\tau_f$ respectively. Both time scales are mathematically analogous and are assumed to be constant in time and ~~space~~also in space for mesoscale domains. When the time scales are set to zero, the maximum precipitation is almost one order of magnitude larger compared ~~with~~ to a configuration with, for example, $\tau_f = \tau_c = 1000$ s (Kunz, 2011). ~~The source term $S$ describes the mass flux of precipitation caused by orographic lifting. For positive $S$, $q_c\tau_c^{-1}$ acts as a source in Eq. (??) and as a sink in Eq. (??). This term is proportional to the cloud water density integrated vertically from the bottom to the top of the lifting area. In light of this fact, it is assumed that the whole column is saturated in the case of lifting. The loss of hydrometeors, $q_h\tau_f^{-1}$ in Eq. (??) is proportional to the hydrometeor column density and determines the precipitation rate $R$. However, in the case of descending air with negative $S$ downstream of mountains, evaporation occurs, and $R$ may become negative.~~

A powerful method for the solution of the advection equations for cloud physics ~~, Eq. (??) and (??), together with the linear theory for~~ together with 3D flow is to apply a two-dimensional (2D) Fourier transform. ~~In Fourier space, the precipitation rate $\hat{R}(k,l)$ is~~ Precipitation at the ground is obtained via an inverse FFT given by the ~~following~~ transfer function:

$$R_{oro}(kx,ly) = \iint \frac{iC_w\sigma\hat{h}(k,l)}{(1-imH_w)(1+i\sigma\tau_c)(1+i\sigma\tau_f)}\cdot e^{i(kx+ly)}\,dk\,dl, \quad (2)$$

which connects the precipitation field in Fourier space ~~, $\hat{R}(k,l)$,~~ (fraction term) to the orography, $\hat{h}(k,l)$, both related to the horizontal wavenumbers $(k,l)$. ~~In Eq. (2), ;~~ $i$ is the imaginary unit, and $C_w = \rho_{S_{ref}}\Gamma_m\gamma^{-1}$ is the uplift sensitivity related to the

condensation rate $\rho_{S_{ref}} = \rho_d q_v$, where $\rho_d$ is the density of dry air, $q_v$ is the water vapor density, and $\Gamma_m$ and $\gamma$ are the moist adiabatic and actual lapse rates~~respectively. Water~~, respectively. The water vapor scale height $H_w$ is the ~~height above ground where the vertical integrated horizontal water vapor flux has reached~~ (absolute) height where the integrated water vapor density dropped to $e^{-1}$~~of its ground value.~~, and $\sigma = Uk + Vl$ is defined as the intrinsic frequency with the components $U$ and $V$ of the undisturbed horizontal wind vector ~~that is~~ assumed to be constant through time and space.

Whereas the nominator of Eq. (2) gives the dependency of precipitation on vertical motion and orography, the first bracket of the denominator describes the ~~relation~~ modification of the source term ~~to~~ by airflow dynamics. The second and third terms of the denominator consider the advection of hydrometeors during the characteristic time scales $\tau_x$ $(x = c; f)$~~and evaporation in the~~. In case of descent ~~,~~ downstream of mountains, $R_{oro}$ may become negative leading to a reduction of total precipitation in Eq. (1) in that area.

~~Vertical~~ The vertical wavenumber $m$ in Eq. (2) is given by the dispersion relation (Smith, 1980):

$$m(k,l) = \left[\frac{N_m^2 - \sigma^2}{\sigma^2}(k^2 + l^2)\right]^{0.5}. \tag{3}$$

In this formulation, $m$ controls both the depth and tilt of forced ascent or descent. Because vertical lifting is assumed to be saturated throughout the whole column, meaning that the lifted condensation level ~~is located~~ (LCL) is directly at the ground, saturated Brunt-Väisälä frequency $N_m$ (e. g., Lalas and Einaudi, 1973) has to be considered instead of the dry one, $N_d$. Compared ~~with unsaturated flow~~to unsaturated conditions, saturated flow leads to a weakening of the amplitude of the gravity waves via the reduction of static stability~~and thus to a flow streaming~~. In this case, the flow tend to go more directly over ~~the mountains~~ an obstacle rather than around ~~as shown, for example, by Durran and Klemp (1982) or Kunz and Wassermann (2011)~~ (Durran and Klemp, 1982; Kunz and Wassermann, 2011). Even though the concept of saturated flow by simply considering $N_m$ must be regarded as an approximation of the reality, it has been successfully applied by several authors studying flow dynamics and precipitation (Jiang and Smith, 2003; Smith and Barstad, 2004; Kunz and Wassermann, 2011).

~~The precipitation field on the ground is obtained via an inverse Fourier transform of the transfer function~~ Combining Eq. (2) ~~:~~

$$R_{oro}(x,y) = \iint \hat{R}(k,l) e^{i(kx+ly)} dk dl .$$

~~Note that $R_{oro}$ can attain negative values meaning a reduction of precipitation totals of superimposed processes. Even though $R_{oro} < 0$ might be mathematically possible, a negative total precipitation does not make sense physically and thus is truncated away. Therefore, we set $R_{tot}(x,y) = \max(R_{tot}(x,y), 0)$ at the end of the summation in (1~~with (3), a total number of seven atmospheric parameters is required as input for $R_{oro}$. In this study, we used vertical profiles of temperature, moisture, and wind from radiosoundings (see Sect. 3.2) for that purpose.

~~The model has five internal free parameters that can be used to adjust/calibrate the model to the observations. Three of these parameters are implicitly considered in the transfer function (Eq. 2) : the two time scales of $\tau_c$ and $\tau_f$, which, however, are virtually identical, and~~

### 2.2.2 Background precipitation

Under the assumption that the prevailing synoptic conditions during the 12 hours of model integration are approximately horizontally homogeneous and stationary, also $R_\infty$ becomes constant. To consider large-scale lifting in the SPM2D, we estimate $R_\infty$ from observed rainfall totals (see Sect. 3.1) over a larger area with almost flat terrain, where $R_{oro}$ as well as evaporation associated with ascent are minimized to a large degree. To ensure proper estimation of $R_\infty$ for the historic events, we choose an area that covers most of the total investigation area, but excludes the Black Forest and the Prealpine region, where precipitation totals are highest. In the selected region (Fig. 2, black box), large totals occur only rarely. Values of more than 50 mm per day, for example, exhibit an annual exceedance probability $p$ of less than 0.5. Furthermore, as confirmed by Fig. 2, the probability of rain totals in excess of 50 mm per day is more or less homogeneously distributed.

## 2.3 Modifications of the SBM

As further development, two types of modifications are applied to the SBM: adjustments to the existing orographic precipitation using additional calibration parameters, and additional precipitation components originating from different physical processes.

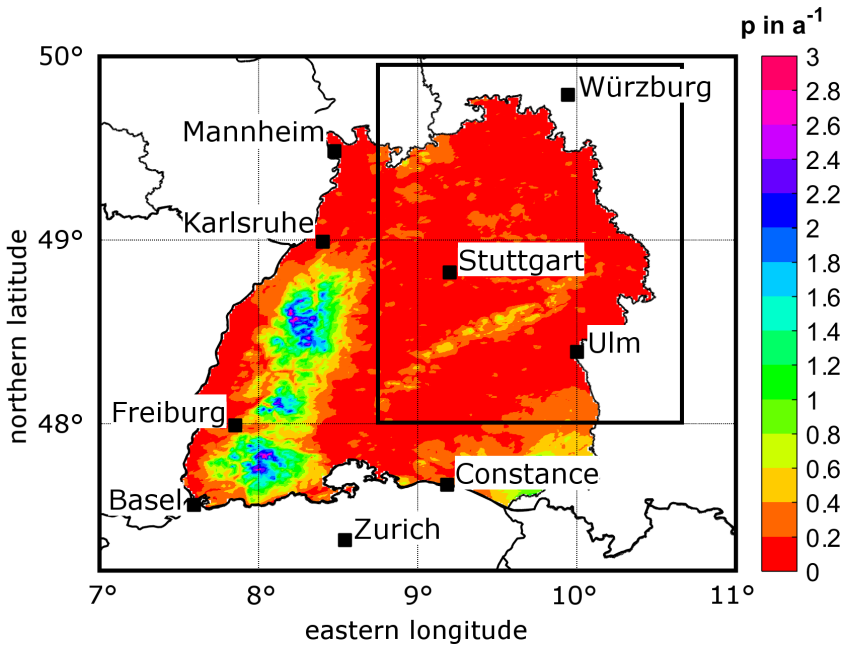


**Figure 2.** Probability of observed 24-hour rainfall totals greater than 50 mm expressed as the average days per year for Baden-Württemberg; the black box indicates the area, where background precipitation $R_\infty$ is estimated.

### 2.3.1 Adjustments to $R_{\mathrm{oro}}$

The original orographic precipitation equation of the SBM (2) is modified in SPM2D by adding three constant calibration parameters (bold symbols):

$$R_{\mathrm{oro}}(x,y) = \boldsymbol{c_{\mathrm{oro}}} \cdot \boldsymbol{f_{\mathrm{dry}}(x,y)} \cdot \iint \frac{i\boldsymbol{f_{\mathrm{C_w}}} C_{\mathrm{w}} \sigma \hat{h}(k,l)}{(1-imH_{\mathrm{w}})(1+i\sigma\tau_{\mathrm{c}})(1+i\sigma\tau_{\mathrm{f}})} \cdot \mathrm{e}^{i(kx+ly)} \mathrm{d}k\mathrm{d}l\,. \tag{4}$$

The uplift sensitivity factor $C_{\mathrm{w}}$ ~~. The latter is modified with a multiplier to $C^*_{\mathrm{w}} = f_{\mathrm{C_w}} \cdot C_{\mathrm{w}}$ with the new factor $C^*_{\mathrm{w}}$ replacing the original $C_{\mathrm{w}}$ in Eq. (2).~~ is adjusted by a multiplier $f_{\mathrm{C_w}}$, which reduces the sensitivity of the ~~model for lifting ,~~ SPM2D for lifting and therefore, the precipitation rate~~is reduced, especially over mountainous terrain with sharp~~ . Precipitation is reduced the most for sharp height gradients, whereas ~~in regions with less orographic gradients~~ the effect is ~~weak~~ only weak for smooth terrain (Fig. 3, red curve). The ~~used model formulation~~ formulation of SPM2D also allows for multiple ascents~~/~~/descents of a virtual air parcel without any ~~change~~ changes in its water vapor content. ~~Actually, water vapor is partly removed~~ The more realistic partial removal of water vapor due to condensation ~~processes during ascent , which is realized by~~ during ascent is also considered by implementing the additional function $f_{\mathrm{C_w}}$.

An additional parameter, $f_{\mathrm{dry}}$, is implemented in Eq. (4) to reduce evaporation in descent regions, where $R_{\mathrm{oro}}$ ~~is~~ becomes negative (Fig. 3, blue curve). The resulting underestimation of precipitation is found especially downstream of steeper moun-

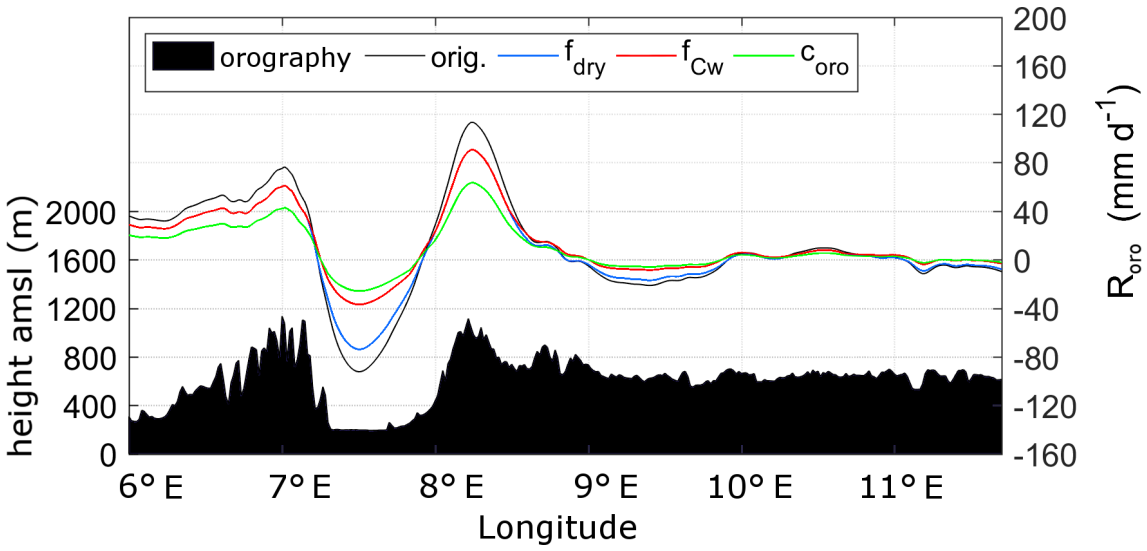


**Figure 3.** Different effects of the implemented internal free parameters $f_{\mathrm{dry}}$ (blue), $f_{\mathrm{C_w}}$ (red) and $c_{\mathrm{oro}}$ (green) on the original orographic precipitation part (black curve) for a ~~west to east~~ west-to-east cross section through the model domain. The underlying orography is shown in black.

tains with greater descent (Kunz, 2011). ~~Parameter $f_{\mathrm{dry}}$ acts only at~~ The parameter $f_{\mathrm{dry}} \leq 1$ only corrects grid points $(x, y)$ where $R_{\mathrm{oro}} < 0$~~, in which $f_{\mathrm{dry}} < 1$ ; in all other cases~~ ; otherwise $f_{\mathrm{dry}} = 1$.

Finally, the last additional calibration parameter, $c_{\mathrm{oro}}$, reduces orographic precipitation in the whole domain (Fig. 3, green curve). It is a consequence of the assumption that the vertical lifting of an ~~entire~~ air column with overall saturation produces condensate and instantaneous fallout at any time, implying an overestimation of precipitable water. In reality, not all layers are completely saturated, and water may also partly be stored by clouds. ~~Parameter~~ The parameter $c_{\mathrm{oro}}$ is ~~implemented similarly to $f_{\mathrm{dry}}$ in Eq. (4) but is~~ assumed to be independent of any lifting processes and constant in time and for the whole domain. ~~With these two parameters, orographic precipitation is modified to:~~

$$R^{*}_{\mathrm{oro}}(x, y) = f_{\mathrm{dry}} \cdot c_{\mathrm{oro}} \cdot R_{\mathrm{oro}}.$$

~~Note again that $f_{\mathrm{dry}}$ affects only grid points with net descent, whereas $c_{\mathrm{oro}}$ is constant over the whole domain.~~ From a mathematical perspective, the two factors, $f_{\mathrm{C_w}}$ and $c_{\mathrm{oro}}$, could collapse to one single parameter. Nevertheless, as mentioned above, they describe modifications ~~on~~ of different physical processes ~~as mentioned in the section above and~~ , ~~hence, have to~~ and must therefore remain separate.

### 2.4 ~~Background precipitation~~

~~The background precipitation term $R_{\infty}$ in Eq. (1) describes the effect of large-scale lifting by synoptic-scale weather patterns. According to the $\omega$-equation, lifting is the result of three different mechanisms: positive vorticity advection increasing with height (or vice versa); the maximum of diabatic phase transitions; and the maximum of warm air advection. Even though lifting is the superposition of these three mechanisms, we do not split $R_{\infty}$ accordingly, as the single forcing terms can not be estimated out of radiosounding data. Furthermore, we assume that the large-scale conditions are almost horizontally homogeneous across the investigation area, and so is $R_{\infty}$ at each time step.~~

~~To simplify the inclusion of large-scale lifting in the SPM2D, we estimate $R_{\infty}$ from observed rainfall totals (see Sect. 3.1) over a larger area with almost flat terrain, where $R_{\mathrm{oro}}$ as well as evaporation by ascent are minimized to a large degree. However, an analysis of various past events shows the strong variability of the spatial distribution of precipitation even over flat terrain. For example, some events affect only the northern parts of the investigation area, whereas other occur only in the southern parts. To ensure a proper estimation of $R_{\infty}$, we choose an area that covers most of the total investigation area but excludes the Black Forest and prealpine lands. In the region, where we estimate $R_{\infty}$ (Fig. 2, black box), heavy rainfall is very unlikely. Totals of more than 50 mm per day, for example, exhibit an annual exceedance probability $p$ of less than 0.5. Furthermore, as confirmed by Fig. 2, the probability of rain totals in excess of 50 mm per day is more or less homogeneously distributed. On average over 66 years, it can be assumed that precipitation in the area used for $R_{\infty}$ estimation mainly results from large-scale lifting and to a lesser extent from orographic influences. Probability of observed 24-hour rainfall totals greater than 50 mm expressed as the average days per year for Baden-Württemberg; the black box indicates the area, where background precipitation $R_{\infty}$ is estimated.~~

### 2.4 ~~Frontal precipitation~~

#### 2.3.1 Frontal precipitation

Apart from large-scale lifting connected to low-pressure systems or waves in the flow patterns, precipitation is also substantially enhanced by synoptic-scale weather fronts. Active fronts may increase precipitation considerably due to cross-frontal circulations and lifting in the warm sector of a cyclone (e. g., Bergeron, 1937; Eliassen, 1962). Conversely, if a front affects only parts of the investigation area (e.g., in case of a trailing front, where the flow is almost parallel to the ~~frontal alignment~~isobars), regions ~~outside the sphere of influence may~~ not affected by the front experience much less or even no rain at all. Both effects are considered by ~~implementing an additional quantity~~ a simplified parameterization $R_{\mathrm{front}}$ in Eq. (1):

$$R_{\mathrm{front}} = (R_{\mathrm{oro}} + R_{\infty}) \cdot (c_{\mathrm{front}} - 1)\,, \tag{5}$$

where $c_{\mathrm{front}}$ serves as ~~the~~ an enhancement or reduction factor of the overall precipitation. In this ~~simple~~ parameterization, $R_{\mathrm{oro}}$ is considered again because frontal precipitation is additionally enhanced by orography as shown, for example, by Browning et al. (1975) or Houze and Hobbs (1982). Due to the additive superposition of all precipitation components in Eq. (1), we have to subtract the original precipitation totals leading to a total multiplier of $(c_{\mathrm{front}} - 1)$.

In order to estimate $c_{\mathrm{front}}$ from the observational data, we define this quantity as the relative difference between observations $O$ and output $M$ of the SBM. This is expressed by

$$c_{\mathrm{front}} = \overline{O} \cdot \overline{M}^{-1} \tag{6}$$

assuming that the differences originate primarily from frontal effects. For the quantification of $c_{\mathrm{front}}$, we use spatial mean values over the investigation area $\overline{O}$ and $\overline{M}$ for a training sample of historic heavy rain events (see Sect. 2.4.1).

The frontal enhancement factor is a function of space realized by a rectangular area ~~$c_{\mathrm{front}}(x, y)$~~$c_{\mathrm{front}}(n, t)$, where the orientation of the ~~$y$~~front-parallel $t$-axis compared to the zonal-orientated y-axis is prescribed by the mean wind direction $\beta$ (Fig. 4).

For each time step the maximum value of $c_{\mathrm{front}}$ is estimated using the corresponding pdf (c. f. Sect. 5.1). To avoid strong gradients at the ~~border areas~~ borders of the rectangular, we applied Gaussian-shaped smoothing~~. Along the $x$-dimension~~: Along the front-normal $n$-axis, the spread is set to $8\sigma_{\mathrm{n}}$, where $\sigma_{\mathrm{n}}$ is the standard derivation of the normal distribution~~. In the $y$~~; in the $t$-direction, ~~an infinitesimal length is considered~~ the front is infinitely extended (Fig. 4). As the minimum of $c_{\mathrm{front}}$ is zero, $R_{\mathrm{front}}$ can also attain negative values, ~~thus~~ leading to a weakening of total precipitation ~~in an area affected or not affected~~ for areas unaffected by a front. ~~In order to calculate $c_{\mathrm{front}}$ from the observational data, we define this quantity as the relative difference between observations $O$ and output $M$ of the rSPM (neglecting embedded convection as described in the next paragraph). This is expressed by~~

~~$c_{\mathrm{front}} = \overline{O} \cdot \overline{M}^{-1}$~~

~~assuming that the differences originate primarily from frontal effects. For the quantification of $c_{\mathrm{front}}$, we use spatial mean values over the investigation area $\overline{O}$ and $\overline{M}$ for a training sample of historic heavy precipitation events (see Sect. 2.4.1).~~

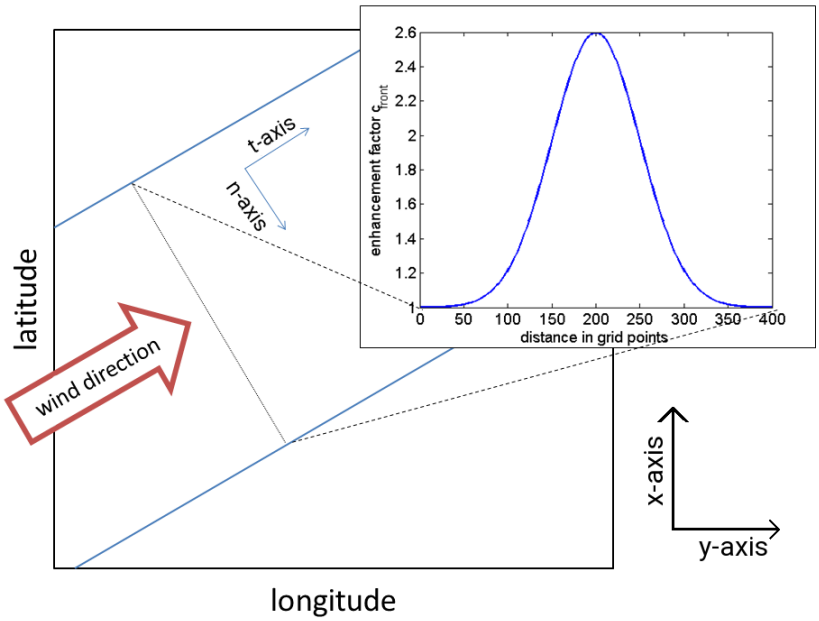


**Figure 4.** Schematic of a Gaussian-shaped distribution of the frontal enhancement factor with a maximum of $c_{\mathrm{front}} = 2.6$ and $\sigma_{\mathrm{n}} = 50$ (upper right corner) and its location in the model domain for a southwesterly wind direction (arrow). The blue lines indicate the boundaries of the frontal zone.

### 2.4 ~~Embedded Convection~~

~~The last part of the total precipitation model SPM2D considers convection embedded in mainly stratiform clouds (e. g., Fuhrer and Schär, 2005). Note, however, that the model is not foreseen to simulate purely convection. Such embedded convection mainly~~

#### 2.3.1 Embedded Convection

Embedded convection mainly occurs when lifting is locally enhanced at mid- and upper tropospheric levels leading to a decrease of thermal stability by the release of ~~the~~ latent heat of condensation (e. g., Kirshbaum and Durran, 2004; Kirshbaum and Smith, 2008; Cannon et al., 2012). Convection in general involves several complex processes that ~~make simulation~~ makes reliable simulations a difficult task. Since our model is restricted to large-scale precipitation with the objective of quantifying extremes ~~in terms~~ of areal precipitation solely, we treat embedded convection in a very simplified way by implementing several rectangular cells as convective footprints similar to the approach ~~of frontal system consideration~~for the fronts.

Because embedded convection is ~~also partly~~ mainly induced by orographic ~~precipitation mechanisms~~lifting, we implemented a multiplicative factor to the precipitation fields related to both orographic and large-scale lifting, similar to the frontal part:

$$R_{\mathrm{conv}} = c_{\mathrm{conv}} \cdot (R_{\mathrm{oro}} + R_{\infty}), \tag{7}$$

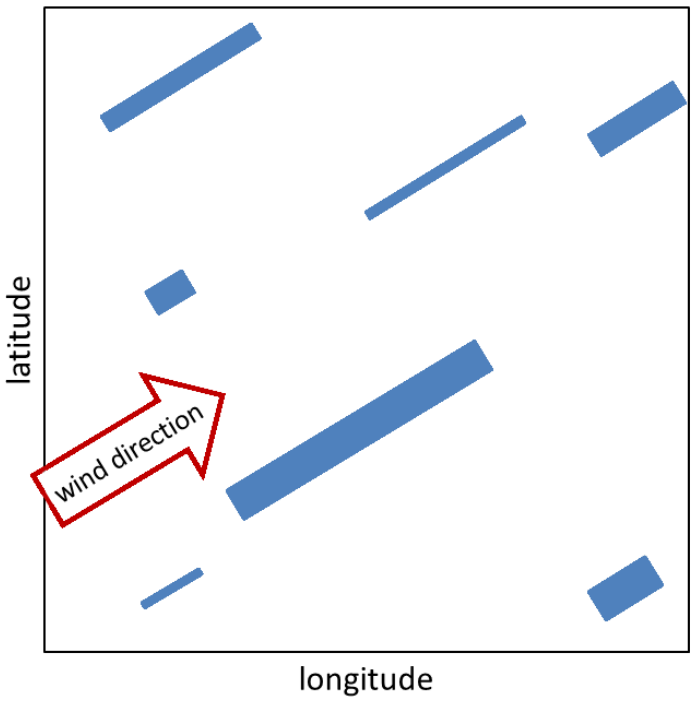


**Figure 5.** Schematic of embedded convection implementation by using rectangular cells (blue). The orientation is defined by the wind direction (arrow); each cell is assigned to an individual factor $c_{\mathrm{conv}}$.

with the enhancement factor $c_{\mathrm{conv}}$.

~~For each time step of the simulation~~ For each 24-hour simulation period, we choose a number of ~~convective cells~~rectangular convective footprints, each with ~~specific~~ a specified width $W$ and length $L$, and distribute them randomly over the whole model domain (Fig. 5). ~~Both width $W$ and length $L$ of each rectangle of the convective cells~~ The dimensions for each rectangle are estimated from the ~~characteristics of the severe convective storms identified from radar data by Fluck, 2018~~ pdfs of historic footprints of deep moist convection (see Sect. 3.3). Furthermore, we restricted the two parameters to $L > W$ and $L_{\mathrm{max}} = 300\,\mathrm{km}$, or 300 grid points, respectively. As for the frontal systems, the wind direction defines the orientation of the longer sides of the rectangles. For each ~~convective cell~~footprint, we choose ~~$L \cdot W$~~ $L \cdot W$ specific factors $c_{\mathrm{conv}}$ with $c_{\mathrm{conv}} \in \{0; 1\}$. As found, for example, by Fuhrer and Schär (2005) or Cannon et al. (2012), embedded convection can enhance precipitation up to 200 %~~; thus,~~, but only locally. Thus, the given range of $c_{\mathrm{conv}}$ is adequate. Within the single ~~cells~~rectangles, the spatial distribution of $c_{\mathrm{conv}}$ randomly varies between the given limits ~~. Summing up all cells enables the existence of more than one cell per day at a specific grid point~~to account for the high spatial variability of convective precipitation.

As embedded convection occurs several times a day and at several locations, we used a variable number of convective footprints in the model. The complete convective precipitation field for each time step is spatially smoothed to avoid sharp

gradients. ~~In contrast to the Gaussian shape smoothing due to a more or less continuous increase/decrease of precipitation enhancement in the case of fronts, we use~~ For this, we applied a moving average ~~with a span~~ of 10 grid points to preserve the high spatial variability of convection. ~~Schematic of the convection implementation with rectangular cells (blue). The orientation is defined by the wind direction (arrow); each cell is assigned to an individual factor $c_{\mathrm{conv}}$.~~

## 2.4 ~~Event definition~~ Pre-Preparations and ~~statistical distribution functions~~Simulation Procedure

### 2.4.1 Event definition and statistical distribution functions

Stochastic modeling of precipitation events with the SPM2D ~~requires the adjustment of appropriate probability density functions (pdfs ) to~~ is based on appropriate pdfs of all input parameters required by the model. These pdfs are estimated ~~from~~ using an adequate set of representative past heavy rainfall events. ~~Based on the pdfs, several thousands events can be stochastically generated.~~ Because the characteristics of the ambient conditions and thus the precipitation regimes change throughout the year, we seasonally differentiate the estimated pdfs ~~among spring (MAM~~between spring (March-April-May, MAM from hereon), summer (June-July-August, JJA), autumn (September-October-November, SON), and winter (December-January-February, DJF).

In the first step, a sufficient and appropriate subset of relevant historic events ~~has been identified. An event here~~ was identified. Here, an event is defined as a period of one or more days with ~~persisting~~ persistent precipitation above a certain threshold of daily ~~precipitation. Because our study focuses on major large-scale flood events and not on local-scale floods or flash floods, an~~ totals. An extension to multi-day events is reasonable to consider time delays in discharge response or flood waves traveling along river networks (e. g., Duckstein et al., 1993; Uhlemann et al., 2010; Schröter et al., 2015).

We define the historic event set ~~based on~~ according to maximum areal precipitation. For this, we simply accumulate the (equidistant) 24-hour rainfall totals $\overline{R}_{\mathrm{BW}}$ of all grid points in ~~BW (~~the investigation area (BW; see Sect. 3.1). Following the sorting of all values of $\overline{R}_{\mathrm{BW}}$ in descending order, the strongest 200 values enter the sample (top200). As precipitation is not limited to these (single) days but may be embedded in longer time periods, we define the threshold $R_{\mathrm{thres}}$ for the event definition. ~~Estimating~~ For estimating $R_{\mathrm{thres}}$, we consider "wet" days by using $\overline{R}_{\mathrm{BW}} > 0$ solely, and set $R_{\mathrm{thres}}$ to the 75 % percentile of this sub-sample. A lower threshold leads to an over-interpretation of longer clusters, a higher one avoids multi-day events.

Event precipitation starts on the first day that exceeds $R_{\mathrm{thres}}$. When areal means of consecutive days are also above $R_{\mathrm{thres}}$, they are simply accumulated, yielding events of more than one day. The last day with $R \geq R_{\mathrm{thres}}$ before a period of at least three days of non-exceedance defines the end of an event. Such a three-day period ensures statistical independence of the events in accordance with the approach of Palutikov et al. (1999) for wind storms. Following Piper et al. (2016), we only count "rain days" ($\overline{R}_{\mathrm{BW}} \geq R_{\mathrm{thres}}$) and neglect "skip days" ($\overline{R}_{\mathrm{BW}} < R_{\mathrm{thres}}$) in between the start-day/end-day period for event duration estimation, which is a widely used approach (Wanner et al., 1997; Petrow et al., 2009). This approach avoids the over-interpretation of longer clusters.

~~Based on the proceduredescribed above~~Based on this procedure, a defined precipitation event contains one or more days of the top200 sample. For this event set, all required input parameters were extracted from sounding data and rainfall totals (see Sect. 3).

In the next step, we identified the pdfs most appropriate for statistically describing each of the seven atmospheric input parameters, event duration $t_{\mathrm{ev}}$, background precipitation $R_{\infty}$ and front factor $c_{\mathrm{front}}$. In addition to 20 pdfs preset by the MATLAB statistic toolbox (MATLAB, 2016), we considered the circular von-Mises distribution (Mardia and Zemroch, 1975) for wind direction only. In ~~total, 17 pdfs were suitable , and tested and compared with the distribution of each parameter for each of the four seasons (Table A1). Note that Gumbel (GbD) and Weibull (WbD) distributions are special cases of the generalized extreme value distribution (GEV) and that some pdfs cannot be used for every parameter due to their ranges of validity. List of the tested and suitable pdfs preset in the MATLAB statistical toolbox (the short acronyms in brackets are for further orientation). Birnbaum-Saunders (BSD) Nakagami (NkD) Gamma (GmD) Normal (ND) Generalized Extreme Value (GEV) Poisson (PD) Gumbel (GbD) Rayleigh (RyD) Half-Normal (HND) Rician (RcD) Inverse Gaussian (IGD) Stable (SD) Logistic (LD) Student's t (StD) Log-Logistic (LLD) Weibull (WbD) Log-Normal (LND)~~ Sect. 5 it will be further discussed which pdfs are most suitable for the input variables in our case.

To find the pdf that best fits the data, we estimated the appropriate number of histogram classes according to Freedman and Diaconis (1981), and ~~we calculated the~~ calculated bias, root mean square error (rmse) and Spearman correlation coefficient $r_{\mathrm{Sp}}$ (Spearman, 1904) as quality indicators (QIs). We also applied a $\chi^2$-test ~~according to Wilks (2006)~~ (Wilks, 2006) as a QI. For each QI, we ranked the pdfs in ascending order and added up the rank numbers for each pdf, receiving the best fit in terms of the least QI–rank sum (QIRS). In the case of alikeness of two or more pdfs (about 10 % of all cases), we manually selected the best one.

### 2.4.2 General Simulation Procedure

The presented SPM2D is an event-based model in the sense that a specified number $n_{\mathrm{E}}$ of independent events with variable duration $t_{\mathrm{ev}}$ is simulated. The general procedure is as follows (cf. Fig. 6): Starting with the iteration loop over $n_{\mathrm{E}}$ events, the season and duration $t_{\mathrm{ev}}$ are set at first. The next step is the simulation of the four precipitation components according to Eq. (1); because radiosoundings used as input data are available every 12 hours, $R_{\mathrm{oro}}$ and $R_{\infty}$ are computed for the same period. In contrast, $R_{\mathrm{front}}$ and $R_{\mathrm{conv}}$ are calculated only for 24 hours as they become apparent as footprints in daily totals. The resulting total precipitation $R_{\mathrm{tot}}$ has a temporal resolution of 24 hours. Despite the fact that the characteristic time scales may vary from one situation to another, it is found that simulations using fixed values for the free parameters yield trustworthy results (e. g. Barstad and Smith, 2005; Kunz, 2011). Here, we also use constant values illustrated as shaded box in Fig. 6. The direct link between the precipitation components and the corresponding input variables (described by appropriate pdfs) is also shown in Fig. 6. In case $t < t_{\mathrm{ev}}$, the next 24-hour period is simulated; otherwise, the loop jumps to the next event. A method how to assign the $n_{\mathrm{E}}$ events to a specific time period, which is required, for example, for insurance purposes, will be introduced in Sect. 6.

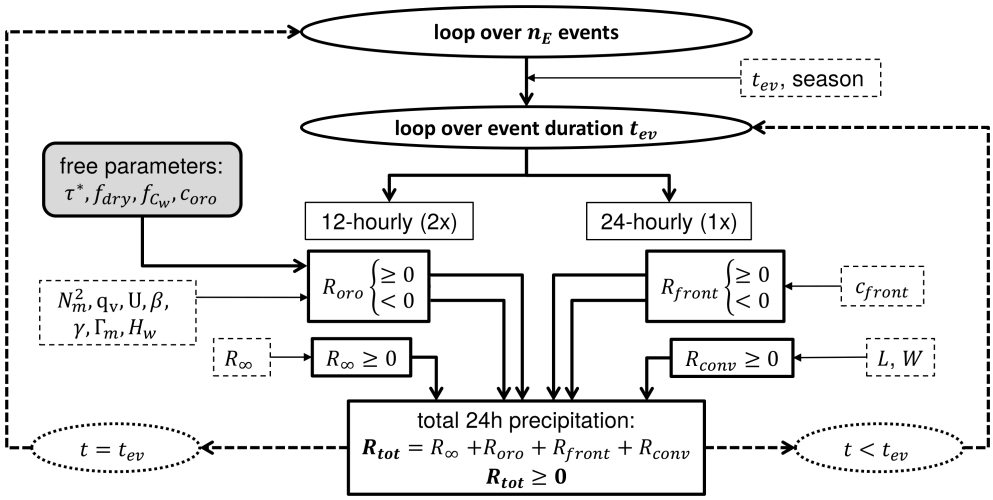


**Figure 6.** Flow chart of the individual components of the SPM2D (solid boxes) and the corresponding input variables (pdfs; dashed boxes). Loops are highlighted as ellipsis or bold dashed arrows. The constant model parameters are illustrated as shaded box.

## 3 Data sets

The SPM2D presented in this study is based on two different types of data sets: gridded precipitation data ~~to estimate background precipitation and to~~ also used to calibrate and verify the model, and vertical profiles from radiosondes to initialize the model. Furthermore, the SPM2D is also validated ~~with reanalysisdata done with the regional climate model of the Consortium for Small Scale Modeling (COSMO-CLM). Unless otherwise indicated, the investigation period covers the years of 1951–2016 (hereinafter referred to as IP).~~ using reanalysis.

### 3.1 Rainfall totals

Rainfall statistics in our study are based on the ~~REGNIE (German: *REGionalisierte NIEderschläge;* regionalized precipitation ) data set~~ regionalized precipitation (REGNIE) data provided by the German Weather Service (~~Deutscher Wetterdienst;~~ DWD). REGNIE is a gridded data set of 24-hour totals (06 to 06 UTC) based on several thousand climate stations more or less evenly distributed across Germany (so-called RR collective). The REGNIE algorithm interpolates the observations to a regular grid of ~~approximately~~ 1 km$^2$ considering elevation, exposition, and climatology (Rauthe et al., 2013). ~~The REGNIE domain covers the area with 5.83° E $\leq \phi \leq$ 16° E and 47° N $\leq \theta \leq$ 55.08° N ($\phi$: longitude; $\theta$: latitude). Grid points outside of Germany are set to a missing value. The observation period is from 06 to 06 UTC.~~

~~It should be noted that REGNIE data are temporally not homogeneous due to~~ Despite of continuous changes in the ~~locations and number of rain gauges. Furthermore~~number of stations considered and several station relocation, REGNIE is sufficiently homogeneous for our purposes. However, areal precipitation exhibits a certain bias especially over elevated terrain, such as

the ~~Black Forest mountains, because~~ peaks of Black Forest, where the number of stations ~~considered by the regionalization is limited. Its magnitude, however, cannot be directly estimated from the observations~~ is very limited (Kunz, 2011).

~~We use the REGNIE data set for the definition of the~~ In our study, we use REGNIE data between 1951 and 2016 to identify the top200 ~~data set , event duration , background precipitation and~~ event set (see previous section), to estimate the duration of the events, the front factor $c_{\mathrm{front}}$, and background precipitation as well as for the validation of the SPM2D simulation results.

### 3.2 Radiosoundings

~~Input of the SPM2D are seven atmospheric parameters derived from radiosoundings: thermal stability in terms of saturated Brunt-Väisälä frequency $N_{\mathrm{m}}$ (e. g., Lalas and Einaudi, 1973) and actual and saturated vertical temperature gradients ($\gamma$ and $\Gamma_{\mathrm{m}}$), water vapor scaling height $H_{\mathrm{w}}$, water vapor mixing ratio $q_{\mathrm{v}}$, wind speed $U$, and direction $\beta$~~ The seven input parameters (see Sect. 2) ~~. These parameters are computed from the vertical profiles~~ required by the SPM2D model are derived from vertical profiles (00 and 12 UTC) of temperature, moisture, wind speed, and direction at the radiosounding station of Stuttgart ~~(48.83° N 9.20° E)~~ located somewhat downstream of the northern Black Forest~~mountains~~. Even though the location might not be ideal because the profiles do not represent undisturbed conditions, the profiles are similar to ~~that~~ those of the upstream station of Nancy in France as shown by Kunz (2011) for heavy rainfall events on average. Data from Nancy ~~, however,~~ are available after 1990 only and, thus, cannot be used in this study, whereas soundings from Stuttgart are available since 1957. ~~We used the soundings at the main standard times for synoptic observations (00 and 12 UTC).~~

~~Sounding data were~~ The vertical profiles, provided by the Integrated Global Radiosonde Archive (IGRA) ~~for quality-controlled radiosonde and pilot balloon observations~~ from the National Climatic Data Center (Durre et al., 2006)~~. These data, available at both main pressure levels and levels of significant changes of one of the parameters,~~ , were interpolated into equidistant increments of $\Delta z = 10$ m (Mohr and Kunz, 2013). All ~~parameters derived from the soundings~~ derived environmental parameters refer to the lowest 5 km of the atmosphere since this layer is most relevant for air flow and stability. Furthermore, to account for the decreasing impact of higher atmospheric layers on the flow characteristics, ~~all~~ the flow parameters $\Lambda$ ~~have been vertically integrated~~ are integrated vertically ($\widetilde{\Lambda}$) ~~, with a~~ applying water vapor weighting ~~being applied~~ (Kunz, 2011):

$$\widetilde{\Lambda} = \frac{\int_{z=0}^{z_{\mathrm{t}}} \Lambda \rho_{\mathrm{d}} q_{\mathrm{v}}\, dz}{\int_{z=0}^{z_{\mathrm{t}}} \rho_{\mathrm{d}} q_{\mathrm{v}}\, dz}, \tag{8}$$

where $\rho_{\mathrm{d}}$ is the density of dry air and ~~$z_{\mathrm{t}} = 5000$~~ $z_{\mathrm{t}}$ is the upper integration limit, here of 5,000 m.

As some layers may be moist-unstable, resulting in imaginary $N_{\mathrm{m}}$, the averaging routine is applied to $N_{\mathrm{m}}^2$. In the few cases, where $\widetilde{N}_{\mathrm{m}}$ was imaginary, it was set to a near-neutral, constant value of 0.0003 $\mathrm{s}^{-1}$.

### 3.3 Parameters for Embedded Convection

~~Embedded convection in the SPM2D is considered by single streaks~~

The stochastic generation of enhanced precipitation ~~(see Sect. ??). These streaks are stochastically generated according to the statistical distributions of the observed maximum length $L$ and width~~ streaks associated with embedded convection, namely their length and width ($L$ and $W$), rely on the statistics of severe convective storms ~~estimated by Fluck (2018)~~in Germany

(Fluck, 2018). In that study, convective storms in Germany, France, Belgium, and Luxembourg between 2005 and 2014 were identified from the constant altitude plan position indicator (CAPPI) for a reflectivity in excess of 55 dBZ~~, also known as the Mason (1971) criterion for hail detection~~. The application of ~~a tracking algorithm based on the concept of the algorithm of~~ the tracking algorithm TRACE3D (Handwerker, 2002) ~~yields entire tracks of convective storms. In total, more than 20~~identified more than 25,000 ~~tracks over Germany, France, Belgium, and Luxembourg were identified during the summer half years (April to September) in the period 2004–2014~~storm tracks. Even though we do not consider rainfall related to severe convective storms ~~or hail~~ in the SPM2D, the statistical distributions of the storm's dimensions are reliable proxies for the extension of enhanced precipitation from embedded convection described by $R_{\mathrm{conv}}$.

### 3.4 Numerical Weather Simulations

~~Simulation results from the~~ The SPM2D ~~are validated with rain totals~~ simulation results are additionally validated with high-resolution reanalysis from the non-hydrostatic Consortium for Small-scale Modeling (COSMO) model in climate mode (CCLM; Rockel et al., 2008). ~~CCLM is run by global~~ Laube (2018) performed a dynamical downscaling of ERA-40 reanalysis from the European Center for Medium-Range Weather Forecasts ~~(ECMWF) with a resolution of T159, which corresponds to approximately 125 km on 60 vertical layers (Kållberg et al., 2004). The ERA-40 is available for the period from September 1957 to August 2002 and includes the assimilation of several observational data sets such as satellite data. Laube (2018) performed a dynamical downscaling of ERA-40 to a~~ (ECMWF; Kållberg et al., 2004) to a horizontal resolution of 2.8 km for Southern Germany using a threefold regional nesting (50, 7, to 2.8 km). High-resolution CCLM data is available for the period 1971–2000. For the evaluation, we considered the top200 REGNIE events, from which around 100 events occurred within the ~~period where CCLM data are available~~ CCLM period including the top two and 7 (14) of the strongest 10 (20) events.

## 4 Calibration

~~This section describes the calibration of the SPM2D by comparing modeled and observed precipitation fields (REGNIE 24-hour totals). The outcome is a combination of the free parameters with the highest skill of the simulated historic rainfall totals (training sample) , which then is used for the stochastic simulations of 10,000 rainfall events (validation sample). The latter is equivalent to a period of several thousand years as described in Sect. 6. At the end of this section a concise study on model sensitivities is given.~~

### 4.1 Method

~~Based on the event set of~~ The SPM2D is calibrated with the top200 ~~, the free model (calibration) parameters , $\tau^*$,~~ events (training data) by adjusting the free model parameters $\tau_x$, $f_{\mathrm{C_w}}$, $f_{\mathrm{dry}}$ and $c_{\mathrm{oro}}$ ~~, are assessed. All other parameters required by the SPM2D~~ (cf. Sect. 2) ~~are quantified from radiosounding profiles at Stuttgart. In this evaluation, the stochastic components of the SPM2D and the randomly modeled components for fronts ($R_{\mathrm{front}}$)~~and ~~embedded convection~~ (comparing the simulation results with observations. The parameter combination yielding the best simulation results are then used for the stochastic

simulations (validation data). The components $R_{\mathrm{front}}$ and $R_{\mathrm{conv}}$ ~~) are neglected. Without these components, the model is~~ are only considered for the stochastic event set and therefore neglected here. In this configuration, the SPM2D is equivalent to the SBM plus our modifications in $R_{\mathrm{oro}}$, referred to as ~~the reduced SPM2D (rSPM)~~SBM+M.

In order to determine appropriate values of the free parameters, a large number of model simulations was carried out~~with the rSPM~~. Whereas one parameter was successively varied, the others were kept constant. The selected ranges and increments of the parameters listed in Table 1 resulted in 2,016 possible parameter combinations, giving a total number of approximately 390,000 simulation days for the top200 event set. ~~For each day and parameter combination, we assess the model skill by quantifying both bias and rmse.~~ Both data sets (~~model output~~ from SBM+M and REGNIE) are slightly smoothed using a running 5×5 grid box ~~. The reason for the smoothing is that REGNIE data , despite having a high resolution of 1 km, exhibit spatial uncertainty due to the limited number of observational data considered.Especially~~ as the REGNIE data show a certain spatial uncertainty (c. f. Sect. 3.1) especially around the crests of Black Forest~~, where the number of stations is very low, REGNIE data cannot reproduce local peak rainfall totals~~. Furthermore, as shown, for example, by Barstad and Smith (2005), smoothed data yield more robust results when comparing model and observation data. Note, however, that larger values of ~~$\tau^*$~~ $\tau_x$ and smaller values of $f_{\mathrm{C_w}}$, respectively, likewise smooth the simulated precipitation fields. In these cases, the QIRS method used for the evaluation (Sect. 2.4.1) has to be applied carefully.

~~To avoid apparently better representations of smoothed data fields, we use skill~~ The model skill was evaluated using the skill score $S$ ~~(~~according to Taylor (2001) (see Eq. A1 ~~) described by Taylor (2001) for evaluating climate models~~ in the Appendix) to determine the best ~~parameter combination of rSPM:~~

$$S = \frac{4\,(1+r)}{\left(\hat{\sigma}_f + \frac{1}{\hat{\sigma}_f}\right)^2 \cdot (1+r_0)},$$

~~where $r$ is the correlation coefficient after Spearman (1904), $r_0$ the maximum attainable correlation, and $\hat{\sigma}_f = \sigma_{\mathrm{mod}} \cdot \sigma_{\mathrm{obs}}^{-1}$ the normalized standard deviation with~~ combination of the free model parameter. $S$ relies on the Spearman (1904) correlation coefficient $r_{\mathrm{Sp}}$ between the SBM+M simulations and the observations (REGNIE) as well as on the standard deviations ~~of~~

**Table 1.** ~~The minimum and maximum~~ Range of values ~~, and the increments~~ of the ~~time scales $\tau^*$, and multiplicative factors~~ free model parameters used for the ~~uplift sensitivity $f_{\mathrm{C_w}}$, the lee-side drying $f_{\mathrm{dry}}$, and the adjustment~~ calibration of ~~orographic precipitation $c_{\mathrm{oro}}$~~the model.

| parameter | minimum | maximum | increment |
|---|---|---|---|
| ~~$\tau^*$~~ $\tau_x$ | 800 s | 1500 s | 100 s |
| $f_{\mathrm{C_w}}$ | 0.5 | 1.0 | 0.1 |
| $f_{\mathrm{dry}}$ | 0.4 | 1.0 | 0.1 |
| $c_{\mathrm{oro}}$ | 0.5 | 1.0 | 0.1 |

~~model output $\sigma_{\mathrm{mod}}$ and observations $\sigma_{\mathrm{obs}}$. For $\hat{\sigma}_f \to 1$ and for $r \to r_0$, $S$ approaches unity, which is the best result. According to Taylor (2001), improved values of rmse or bias do not lead to an actual improvement of the model performance, and the use of correlation and standard deviation is more stable. Furthermore, Taylor (2001) provided no regulation for the estimation of $r_0$. Therefore, we set $r_0$ to the maximum calculated correlation coefficient of all simulations. As it is not guaranteed that this maximum is the actual maximum attainable correlation, we increase $r_0$ by 10 %, yielding $r_0 = 0.93$.~~

~~Skill~~ $\sigma$ of both data sets. The skill score $S$ is computed for each ~~simulation day~~ day of top200 and each parameter combination. From all realizations, we select the parameter combination that yields the highest median value of $S$ averaged over ~~all~~ top200~~events~~, as the SPM2D should be able to properly represent a broad range of different atmospheric conditions.

### 4.2 Calibration Results

Applying the method ~~to the top200 events~~ as described above, the highest ~~median skill score of~~ value for $\mathrm{S} = 0.60$ as the median of all top200 events is obtained for the combination of ~~$\tau^* = \tau_x =$~~ 1400 s, $f_{\mathrm{C_w}} = 1.0$, $f_{\mathrm{dry}} = 0.4$ and $c_{\mathrm{oro}} = 0.8$. For this combination, the median values of the other quality indices are $r_{\mathrm{Sp}} = 0.39$, $\hat{\sigma}_f = 0.98$, bias = 6.30 mm, and rmse = 14.85 mm. The assessed ~~values for the former two model parameters are~~ value for $\tau_x$ is physically plausible and comparable to other studies with the ~~rSPM (e.g., Barstad and Smith, 2005; Caroletti and Barstad, 2010; Kunz, 2011). The latter two parameters are incorporated exclusively in this study. However, considering~~ SBM (e.g., Barstad and Smith, 2005; Caroletti and Barstad, 2010; Kunz, 2011). Considering the slight overestimation of orographic precipitation ~~enhancement~~ and the strong overestimation of lee-side drying ~~, the two values seem to be physically plausible as well.~~

~~The sensitivity of skill score $S$ to $\tau$ and to the two other parameters, $f_{\mathrm{C_w}}$ and $c_{\mathrm{oro}}$ (Fig. **??**), shows a dipole structure in both cases with the highest values~~ of ~~$S$ along a counter diagonal. Minor skill scores are obtained with the shortest (longest) time scales in combination with the highest (lowest) uplift sensitivity or highest (lowest) weighting of $R_{\mathrm{oro}}$ in Eq. (1). This implies, on the one hand, that for smaller displacements of precipitation from the formation region, orographic precipitation is overestimated by the rSPM and thus has to be reduced. On the other hand, $R_{\mathrm{oro}}$ has to increase for wider displacements. Sill score $S$, averaged over the top200 event set, depending on $\tau$ and (a) $c_{\mathrm{oro}}$, and (b) $f_{\mathrm{C_w}}$, while the other free parameters, respectively, were set to their optimum values.~~

the SBM, the values for those adjustments are also physically plausible. Note that the above-identified parameter combination yields the lowest errors only when averaging over all top200 events. Single events ~~may become~~ are more realistic with another parameter combination, reflecting particularly the unknown, and thus not considered microphysical processes that are decisive for precipitation formation ~~and~~ strongly controlled by vertical wind speed, temperature, and moisture profiles. The dependency of microphysical processes on ambient conditions, however, is not relevant when running the model in the stochastic mode as is the objective in this study.

The sensitivity of the skill score $S$ to changes in $\tau$, $f_{\mathrm{C_w}}$, and $c_{\mathrm{oro}}$ (Fig. S1, supplements) shows a kind of dipole structure in both cases with the highest values of $S$ along the counter diagonal. Lower values for $S$ are obtained for the shortest (longest) time scales in combination with the highest (lowest) uplift sensitivity or highest (lowest) weighting of $R_{\mathrm{oro}}$ in Eq. (1).

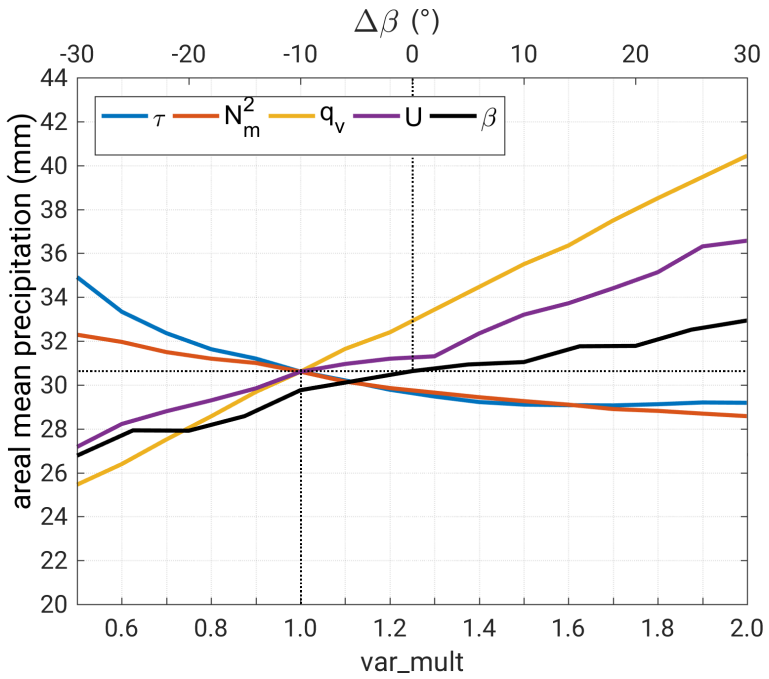


**Figure 7.** Areal mean precipitation (24-hour totals; median of the top200 event set) as a function of $N^2_{\mathrm{m}}$, $q_{\mathrm{v}}$, $U$, $\beta$, and $\tau$ perturbed by a multiplicative factor ($0.5 \leq var\_mult \leq 2$) and changed $\Delta\beta$. The dotted lines indicate the values of the reference run.

This means that horizontal precipitation drift over short distances also reduces evaporation, leading to an overestimation of orographic precipitation (and vice versa). This effect has to be considered by adjusting $R_{\mathrm{oro}}$.

### 4.3 Sensitivity of simulated total precipitation

To demonstrate how variations of atmospheric conditions translate into precipitation, we conduct a sensitivity study with ~~rSPM~~ SBM+M using the top200 event set by gradually changing the values of the input parameters. Following Kunz (2011), we perturbed the values of $N^2_{\mathrm{m}}$, $q_{\mathrm{v}}$, $U$, $\beta$, and $\tau$~~estimated from the top200 events~~. This is done by multiplying the respective quantity with $var\_mult$ increasing linearly from 0.5 to 2.0 in increments of 0.1. Wind direction $\beta$ is varied in the range of $\pm 30°$ in increments of 5°. The calibration parameters are set to their optimum values estimated in the previous section. Besides areal mean precipitation, we ~~analyze~~ computed rmse and skill score $S$ for the median ~~over~~ of the top200 event set.

~~Areal mean precipitation accumulated over 24 hours~~ Mean precipitation shows a high sensitivity to changes in ~~water vapor content~~ $q_{\mathrm{v}}$, ~~wind speed~~ $U$ and ~~wind direction~~ $\beta$ (Fig. 7). In all cases, precipitation increases (decreases) with increasing (decreasing) ~~parameter~~ values. Lowest sensitivity occurs for $\beta$ between $\pm 15°$ because of the orientation of the major orographic structures (~~e. g.~~i.e., the Black Forest) from southwest to northeast. Westerly ~~inflows~~inflow, prevailing on average, still ~~occur~~ occurs for small variations of $\beta$. For greater shifts ($\Delta\beta > 20°$ or $\Delta\beta < -20°$), when the inflow angle becomes smaller, the

sensitivity slightly increases. The changes in the wave regimes and, thus, the location of the updraft may also explain the partly stepwise form of the curves for both $\beta$ and $U$. The results for ~~varying stability~~ $N_{\mathrm{m}}^2$ and ~~microphysical time scales~~ $\tau$ reveal an opposite behavior ~~of areal mean~~ with an increase ~~at~~ of precipitation for smaller values and vice versa. Furthermore, the sensitivity of the ~~model~~ SBM+M to changes of these two parameters is much weaker compared to the other parameters. ~~Areal mean precipitation (median of the top200 BW event set) as a function of $N_{\mathrm{m}}^2$, $q_{\mathrm{v}}$, $U$, $\beta$, and $\tau$ perturbed by a multiplicative factor ($0.5 \leq var\_mult \leq 2$) and changed $\Delta\beta$. The dotted lines indicate the values of the reference run.~~

Qualitatively a similar behavior of the model is found for the medians of rmse and skill score $S$ (Fig. ??S2). While areal precipitation ~~discussed above~~ only provides insights how changes in the ambient parameters feedback into rainfall, rmse and $S$ also consider ~~its~~ the spatial distribution. The results for rmse (Fig. ??S2 a) again reveal the highest sensitivity of the ~~rSPM~~ SBM+M to changes in $q_{\mathrm{v}}$ and $U$. While for $var\_mult > 1$ the sensitivity in terms of rmse is similar to areal precipitation, there is a much higher sensitivity for ~~values below 1.~~ $var\_mult < 1$. In those cases, orographic precipitation is more detached to the mountain crests resulting in higher totals due to reduced evaporation in the descent regions. Because of the combination of higher totals at different locations, rmse show a higher sensitivity to changes of $\tau$ and $N_{\mathrm{m}}^2$ compared to areal mean precipitation.

The skill score $S$, on the other hand, is most sensitive to changes in $q_{\mathrm{v}}$ and $\tau$ (Fig. ??S2 b). Regarding $N_{\mathrm{m}}^2$, $S$ decreases just for very high values of $var\_mult$, while there is almost no sensitivity on ~~the wind direction~~ $\beta$. In all cases, highest $S$ is obtained for the original values of the input parameters~~($var\_mult = 1$ or $\Delta\beta = 0°$), indicating the well calibration of the model . Same as Fig. 7, but for (a) median rmse and (b) median skill score $S$.~~ , confirming that the model is well calibrated.

### 4.4 Case Study

After the parameter adjustment, the ~~rSPM~~ SBM+M tends to slightly underestimate orographic precipitation, whereas totals over flat or rolling terrain are overestimated. This behavior can be seen ~~, for instance, in the example~~ for the case study of 31 May 2013 (Fig. 8), a heavy precipitation event that triggered the severe flooding in 2013 (Schröter et al., 2015).

On that day, a pronounced low pressure system with its center over Croatia led to the sustained advection of moist ~~airmasses~~ air masses from northerly directions around 20° in combination with synoptic-scale ascent. The Stuttgart sounding ~~with~~ showed low stability ($N_{\mathrm{m}} = 0.0055\,\mathrm{s}^{-1}$), high precipitable water ($pw = 24\,\mathrm{kg\,m}^{-2}$), and high wind speed ($U = 20\,\mathrm{m\,s}^{-1}$), ~~the latter two determining the horizontal water vapor flux,~~ which is already an indication of ~~high precipitation totals~~heavy rainfall. Consequently, precipitation totals across the investigation area reached values ~~between 10 and 100~~ of 10–100 mm.

Overall, the ~~rSPM~~ SBM+M is able to reproduce most of the structures of the observed rain field (Fig. 8)~~. The quality indices for that day are $S$ =~~, especially the location of the maxima. The observed mean for Baden-Württemberg is $\overline{R}_{\mathrm{obs}}$ = ~~0.62, $r_{\mathrm{Sp}}$ =~~33.1 ~~0.30, $\hat{\sigma}_{\mathrm{r}}$ =~~mm, whereas the simulated mean is $\overline{R}_{\mathrm{mod}}$ = 37.3 ~~0.75, bias~~mm, thus only 12.6 ~~=~~% higher compared to the observations. Maximum values are $R_{\mathrm{max,obs}}$ = ~~4.44~~91.7 mm ~~, and rmse~~and $R_{\mathrm{max,mod}}$ = ~~=~~76.3 ~~14.82~~mm, respectively, which is a deviation of about 17 ~~mm~~%. The area with $R \geq 50$ mm is almost equal with slightly less grid points ($\approx 6$ %) in SBM+M. The best agreement ~~between observed and simulated precipitation fields~~ is found for the Northern Black Forest as well as the Swabian Jura. Over the northern part of the model domain (north of 49° N) and southwest of Stuttgart, simulated rainfall is substantially higher compared with REGNIE. ~~By~~ In contrast, the ~~rSPM~~ SBM+M simulates lower totals in the Southern

Rhine Valley near and over the mountainous regions of the Southern Black Forest (around Freiburg), especially east of the ~~Basel region~~city of Basel, where lee-side evaporation in the model dominates. The quality indices for that day are $S = 0.62$, $r_{\mathrm{Sp}} = 0.30$, $\hat{\sigma}_{\mathrm{f}} = 0.75$, bias $= 4.44$ mm, and rmse $= 14.82$ mm.

One reason for the discrepancy between observed and simulated precipitation might be the ~~ill-suited~~ suboptimal location of the Stuttgart sounding used for the model initialization. The sensitivity study as described in Sect. 4.3 for this particular event obtains the best results in terms of the lowest rmse (Fig. 9) for ~~higher stability (~~an increase of $N_{\mathrm{m}}^2$ ~~) or longer time scales~~or $\tau$, whereas in the case of ~~water vapor density~~ $q_{\mathrm{v}}$ or ~~horizontal wind speed~~ $U$, the lowest rmse is obtained when decreasing the original values. ~~The results also reveal a higher sensitivity of the rSPM to changes in water vapor and wind speed for this event. Regarding wind direction~~ Regarding $\beta$, the lowest rmse is given for the original value.

The highest skill score $S$, conversely, is reached for increasing $U$ and $q_{\mathrm{v}}$, and decreasing $\tau$ and $N_{\mathrm{m}}^2$. In the case of ~~wind direction~~$\beta$, $S$ continuously decreases from 0.8 ~~in the~~ for northwesterly inflow to 0.4 ~~in the~~ for northeasterly winds.

~~For the case study of 31 May 2013, the observed mean for Baden-Württemberg is $\bar{R}_{\mathrm{obs}} = 33.1$ mm, whereas the simulated mean is $\bar{R}_{\mathrm{mod}} = 37.3$ mm, and thus, only 12.6 % higher compared with the observations. The rmse and skill score $S$ are near the optimum when perturbing different variables. The deviations of spatial means and quality indices are at a reasonable level. However, as already explained, the SPM2D is not designed to represent historic events in detail. Other parameter combinations of $f_{\mathrm{C_w}}$, $f_{\mathrm{dry}}$, $c_{\mathrm{oro}}$ and $\tau^*$ may yield even better results for this single event.~~

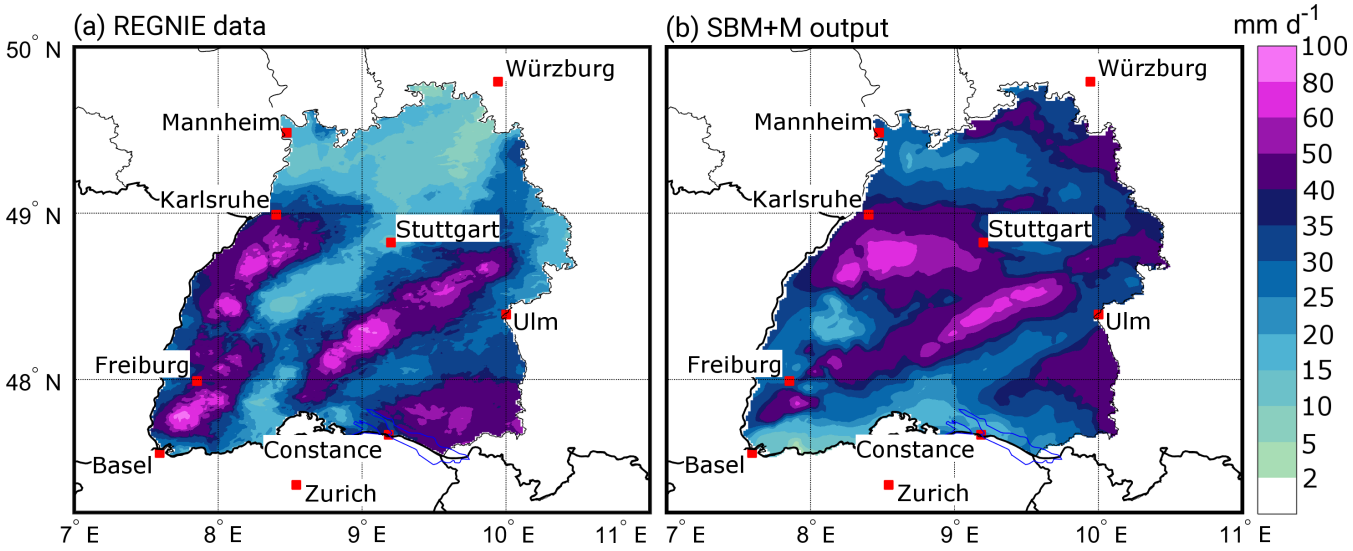


**Figure 8.** Comparison of (a) REGNIE 24-hour rainfall totals, and (b) ~~rSPM~~ SBM+M output for Southwest Germany, exemplary on 31 May, 2013. Note that REGNIE data are available for Germany only. The parametrization in (b) is ~~$\tau^* =$~~ $\tau_x = 1400$ s, $f_{\mathrm{C_w}} = 1.0$, $f_{\mathrm{dry}} = 0.4$, and $c_{\mathrm{oro}} = 0.8$. The areas outside of Baden-Württemberg are covered white for better visualization and comparison.

## 5 Parameter estimation ~~for~~ of the stochastic simulations

### 5.1 Adjustment of the ~~distribution functions~~pdfs

~~Stochastic model simulations are based on pdfs that are adjusted to the required parameter. Event duration as well as background and frontal precipitation are estimated from REGNIE data for the top200 event set. Ambient parameters required by the SPM2D are derived from vertical profiles of the radiosondes at Stuttgart, whereas the extent of embedded convection is estimated from~~

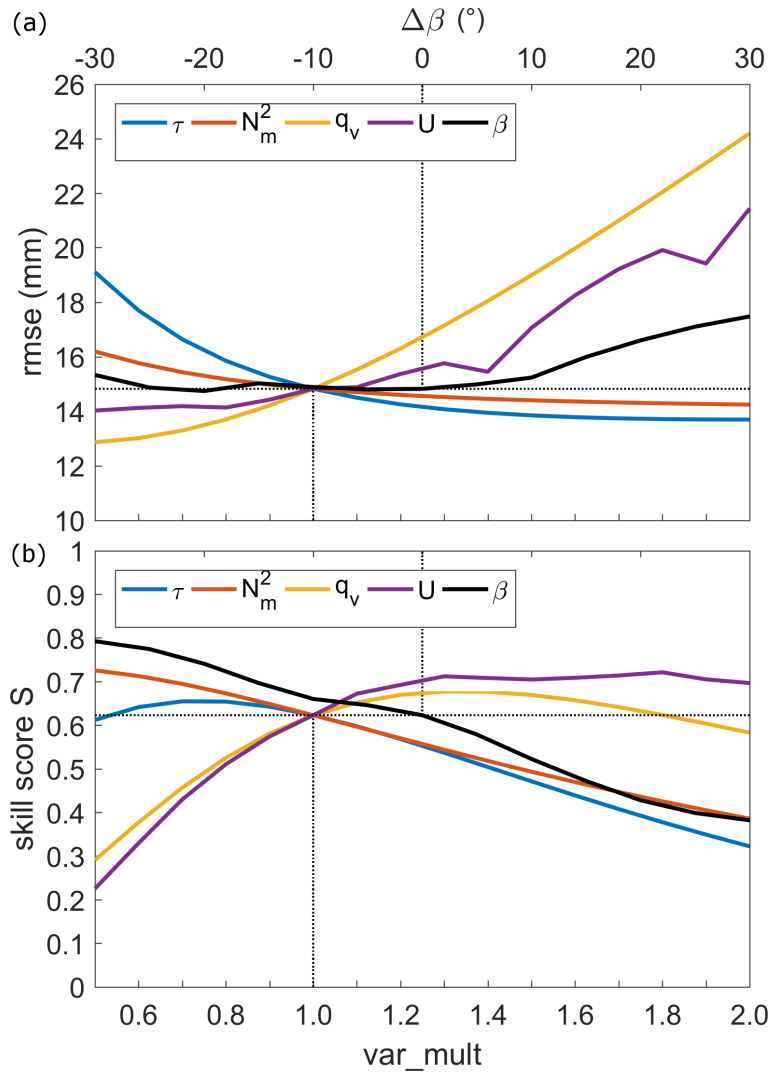


**Figure 9.** Changes of (a) rmse, and (b) skill score $S$ for perturbed values of $N_{\mathrm{m}}^2$, $q_{\mathrm{v}}$, $U$, $\beta$, and $\tau$, with a multiplicative factor ($var\_mult$), and changed $\Delta\beta$, for 31 May, 2013. The dotted lines indicate the values of the reference run.

~~the radar tracks of severe convection. Furthermore, as mean ambient conditions and thus precipitation characteristics change throughout the year, we differentiate among the four seasons.~~

After separating the historic event set into the four main seasons, we estimate for each of the 10 input parameters the pdf that best fits the distribution of the observations (~~= 10 parameters × 4 seasons = 40 cases;~~ Table 2) by using the least QIRS method (cf. Sect. 2.4.1). From the overall 21 pdfs that were considered, only 12 ~~are~~ turned out to be suitable for adjusting the observations. In most of the cases, the ~~GEV~~ generalized extreme value distribution (GEV) with its special realizations of Gumbel (GbD) and Weibull (WbD) distribution appears to be appropriate (26 ~~distributions~~cases), followed by the inverse Gaussian ~~pdf~~ (IGD) for five parameters and the Gamma ~~pdf~~ distribution (GmD) for three parameters. Especially for flow parameters derived from the soundings, the GEV appears to be the most appropriate (19 out of 28 cases). ~~In five out of 40 cases (≈ 12.5 %), we~~ We had to choose the pdf manually five times due to the alikeness of two pdfs according to the QIRS method.

The input parameters are considered as independent and uncorrelated. To justify this assumption, we ~~perform~~ performed a correlation analysis of all possible combinations of input parameters using the ~~correlation coefficient of Spearman (1904). In total, a~~ Spearman (1904) correlation coefficient. A low number of about 16 % of the parameters have a correlation coefficient above $\pm 0.5$, and only 4 % are highly correlated with $\pm 0.7$. Regarding these cases, 90 % show negative correlations with $r \leq -0.5$. However, there are distinct seasonal differences~~, for instance, with correlations in summer, but almost no correlation in winterregarding the same variables. The most frequent~~ ; in some cases correlations are higher in summer than in winter. The highest correlation exists between ~~the saturated Brunt-Väisälä frequency~~ $N_\mathrm{m}^2$ and the lapse rates~~$\gamma$ and $\Gamma_\mathrm{m}$. Furthermore,~~

**Table 2.** Estimated best fitting pdfs for event duration ($t_\mathrm{ev}$), background precipitation $R_\infty$, and frontal enhancement factor $c_\mathrm{front}$ derived from REGNIE data (top box); square of saturated Brunt-Väisälä frequency $N_\mathrm{m}^2$, wind direction $\beta$, horizontal wind speed $U$, water vapor scale height $H_\mathrm{w}$, actual lapse rate $\gamma$, saturated moist adiabatic lapse rate $\Gamma_\mathrm{m}$, and condensation rate $\rho_{\mathrm{S}_\mathrm{ref}}$ derived from sounding data (bottom box); for the pdf aconyms: see Table A1.

| model parameter | MAM | JJA | SON | DJF |
|---|---|---|---|---|
| $t_\mathrm{ev}$ | GEV | GEV | BSD | NkD |
| $R_\infty$ | WbD | WbD | WbD | WbD |
| $c_\mathrm{front}$ | LND | GmD | LND | ND |
| $N_\mathrm{m}^2$ | GEV | GbD | GEV | GEV |
| $\beta$ | GEV | GEV | GEV | SD |
| $U$ | HND | IGD | HND | GEV |
| $\gamma$ | GEV | GEV | IGD | IGD |
| $\Gamma_\mathrm{m}$ | GEV | IGD | IGD | GEV |
| $H_\mathrm{w}$ | GEV | GbD | GEV | LD |
| $\rho_{\mathrm{S}_\mathrm{ref}}$ | WbD | GEV | WbD | WbD |

as shown in Sect. 4,, which is plausible as both are based on the vertical temperature gradient. Because the SPM2D is less sensitive to $N_\mathrm{m}^2$ (c.f. Sect.Thus associated correlations have less influence, 4) the effect can be neglected in the model.

### 5.2 Event characteristics

Based on REGNIE data and the method described in Sect. 2.4.1, we estimate for each event within top200 the duration $t_\mathrm{ev}$ (in days), again differentiating among the seasons. The histogram of historic events the duration $t_\mathrm{ev}$ for the top200 event set and the corresponding best-fitting pdf(, shown exemplary in Fig. 10) shows that during the summer (JJA), illustrated that during JJA, a duration of two to three days dominates with a decreasing probability toward longer periods. In the winter (DJF)During DJF, the distribution is generally shifted to longer events, whereas the probability for single-day events remains roughly unchanged. The maximum of 15 days in DJF represents the longest duration of the top200 event set. Whereas the estimated pdf for the summer JJA (GEV) has a sharper maximum and a stronger decrease for $t_\mathrm{ev} > 3$, the pdf found to best fit the duration in the winter DJF (NkD) shows a broader range of possible durations. Note that the histogram in the winter shows a large scattering with irregular peaks, making an adjustment to a pdf very problematic. For spring and autumnof a pdf difficult. For MAM and SON, the results are comparable to those of winter and summerDJF and JJA, respectively.

Concerning background precipitation $R_\infty$, totals of 20–25 mm d$^{-1}$ are found to most likely occur within a range of 3–37 mm d$^{-1}$ in winterDJF, 3–50 mm d$^{-1}$ in summerJJA, and 0–50 mm d$^{-1}$ during the other two seasons (not shown). For all seasons, the Weibull distribution (WbD) is most appropriate. For frontal factor The corresponding pdfs are listed in Table 2. For the $c_\mathrm{front}$ , we obtain a log-normal distribution (LND) for spring and fall, a normal pdf (ND) for the winter, and a Gamma pdf (GmD) for the summer. All parameter, all pdfs have their maximums maximum around 0.7 to 0.8 with a range from 0.4 to 1.4 for most of the seasons (not shown). The gamma distribution in fall has a sharp ascent and a slower descent toward distribution in SON (Table 2) descends slower towards higher values (maximum of around 1.6).

### 5.3 Atmospheric parameters

As described in Sect. 2, orographic precipitation in the SPM2D depends on seven atmospheric parameters (cf. Table 2). An overview of the range of all parameters the seven input parameters of the model is shown as box plots in Fig. 11; the corresponding pdfs are listed in the bottom box of Table 2. In most cases, the atmosphere was slightly stably stratified as represented by positive values of the squared Brunt-Väisälä frequency $N_\mathrm{m}^2$ affecting the wave propagation. During summerJJA, the distribution is shifted toward negative values (= unstable; recall that negative values are set to $N_\mathrm{m} = 0.0003$ s$^{-1}$), whereas in winterDJF, there are almost entirely positive values. Wind direction $\beta$, decisive for the spatial distribution of precipitation around the mountains, shows pronounced seasonal differences. More than 90 % of the top200 winter DJF events have south-westerly to northwesterly winds (240°–300°), with other directions hardly observed. The reason is that northerly flows are usually associated with low temperatures and thus low humidity during the winter and do not have the potential for heavy precipitation. In summerDJF. In JJA, the wind direction that occurred most frequently is between 240° and 300° as well. However, all other directions have been observed as well.

Horizontal wind speed $U$ in all cases and all seasons is high, especially during ~~winter~~DJF, where reduced moisture is compensated by high velocity to obtain substantial horizontal incoming moisture flow. Median values are 5 and 20 $\mathrm{m\,s^{-1}}$ during ~~summer and winter~~ JJA and DJF, respectively. Flow parameters related to humidity ($H_\mathrm{w}$, $\rho_{\mathrm{S}_\mathrm{ref}}$) conversely show higher values in ~~summer~~JJA, where $\Gamma_\mathrm{m}$ is reduced due to the release of latent heat. ~~Observed vertical temperature gradients~~ The quantity $\gamma$ ~~show~~ shows similar medians and interquartile ranges with a broader distribution in ~~winter~~DJF.

## 6 Stochastic event set and model validation

Overall, a total number of $n_\mathrm{E} = 10{,}000$ events (~~approx.~~ equivalent to approx. 31,500 days) have been simulated with the SPM2D ~~, hereafter referred to as SPM10k.The rSPM part of this event set is referred to as rSPM10k in the following section.~~in stochastic mode (see Sect. 2.4.2). Therefore, a stochastic set of input variables with the same size as the number of simulation days was created using the estimated pdfs, where the variables can be treated as independent (c.f. Sect. 5.1). For the validation of the SPM2D, we quantified statistical ~~values,~~ metrics such as return periods, probabilities, ~~or percentiles and evaluate~~ and percentiles and evaluated them with observations (REGNIE), CCLM simulations and the ~~rSPM results. Note that the main~~

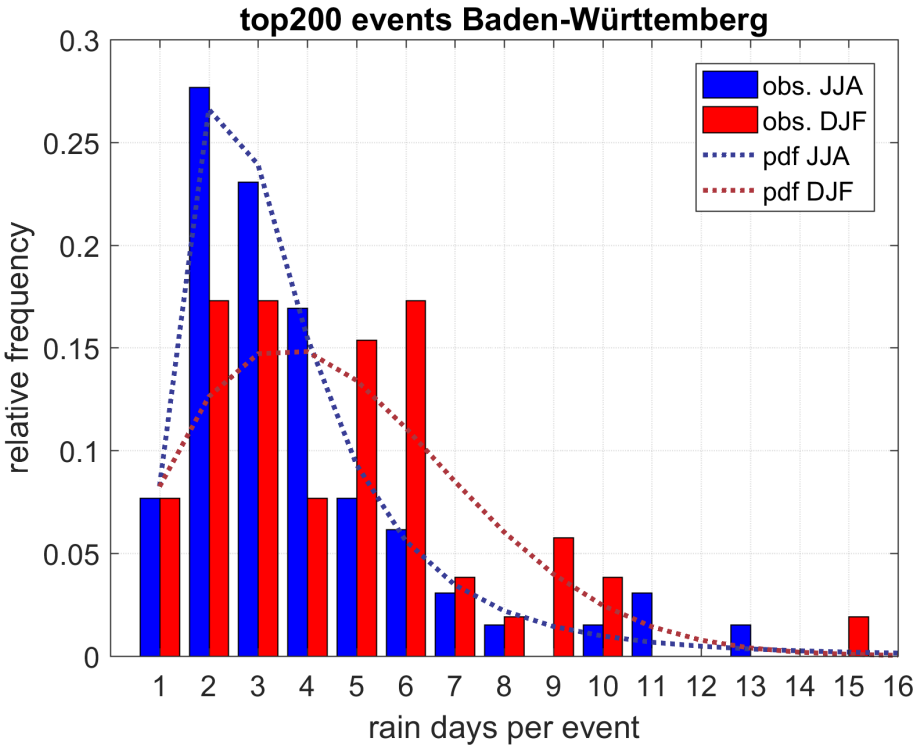


**Figure 10.** Histogram of top200 event duration for Baden-Württemberg according to REGNIE (bars), and estimated best fitting pdfs (dotted lines) for the summer (blue) and the winter (red).

~~reference is the REGNIE~~ SBM+M part. The statistical distribution of the stochastic event set of SPM2D should agree with that of the top200 ~~event set.~~ historic events to a large degree, and more robust results should be notable at the heavy tail (extreme events). The comparison with the SBM+M part is helpful to highlight the quality and necessity of the modifications made to the original SBM. High resolved CCLM simulations are chosen for validation to demonstrate the advantages of a statistical approach for stochastics instead of a dynamical NWP model.

Spatial 24-hour mean values ~~for the area of Baden-Württemberg~~ range between 1.2 and 79.7 mm in SPM2D, and 1.3 to 97.0 mm in ~~rSPM~~SBM+M, whereas the maximum for top200 is only 49.6 mm. In total, 128 events (0.4 %) of ~~SPM10k~~ SPM2D or 724 (2.1 %) of ~~rSPM10k~~ SBM+M yield higher spatial precipitation amounts than the maximum of top200. The CCLM simulations range between 1.8 and 37.6 mm.

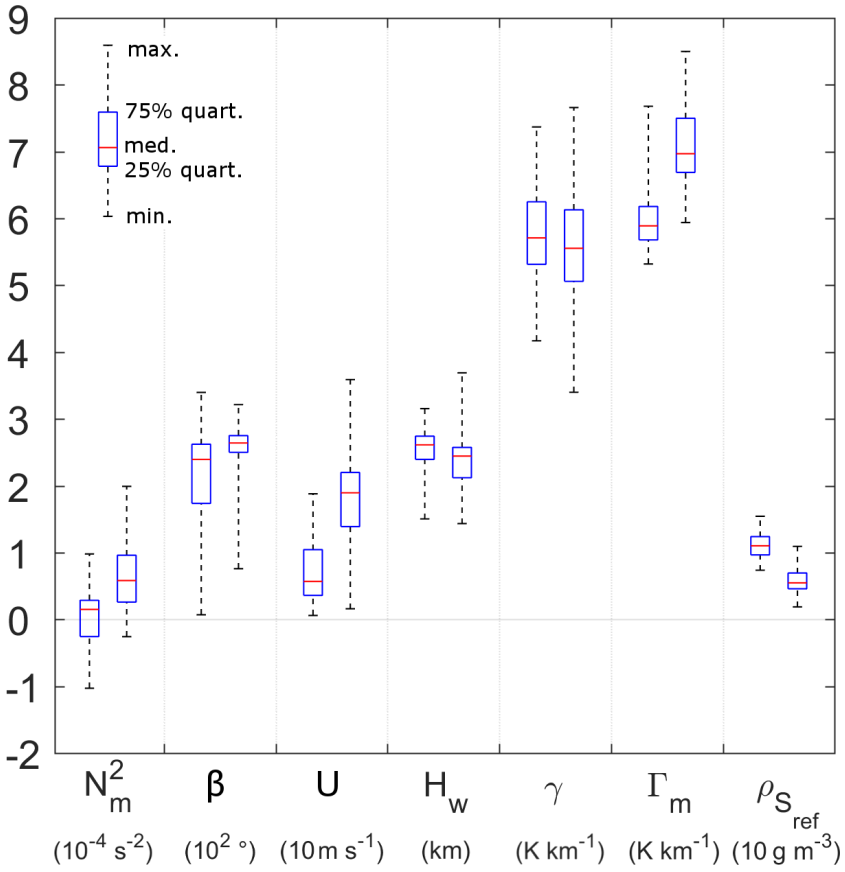


**Figure 11.** Atmospheric parameters required as input for the SPM2D derived from radiosounding observations at Stuttgart for the top200 events with mean, interquartile distance, minimum, and maximum values; the left box-whisker of each pair represents the summer, the right one represents the winter season. The units for each variable are given in the brackets below the variable names.

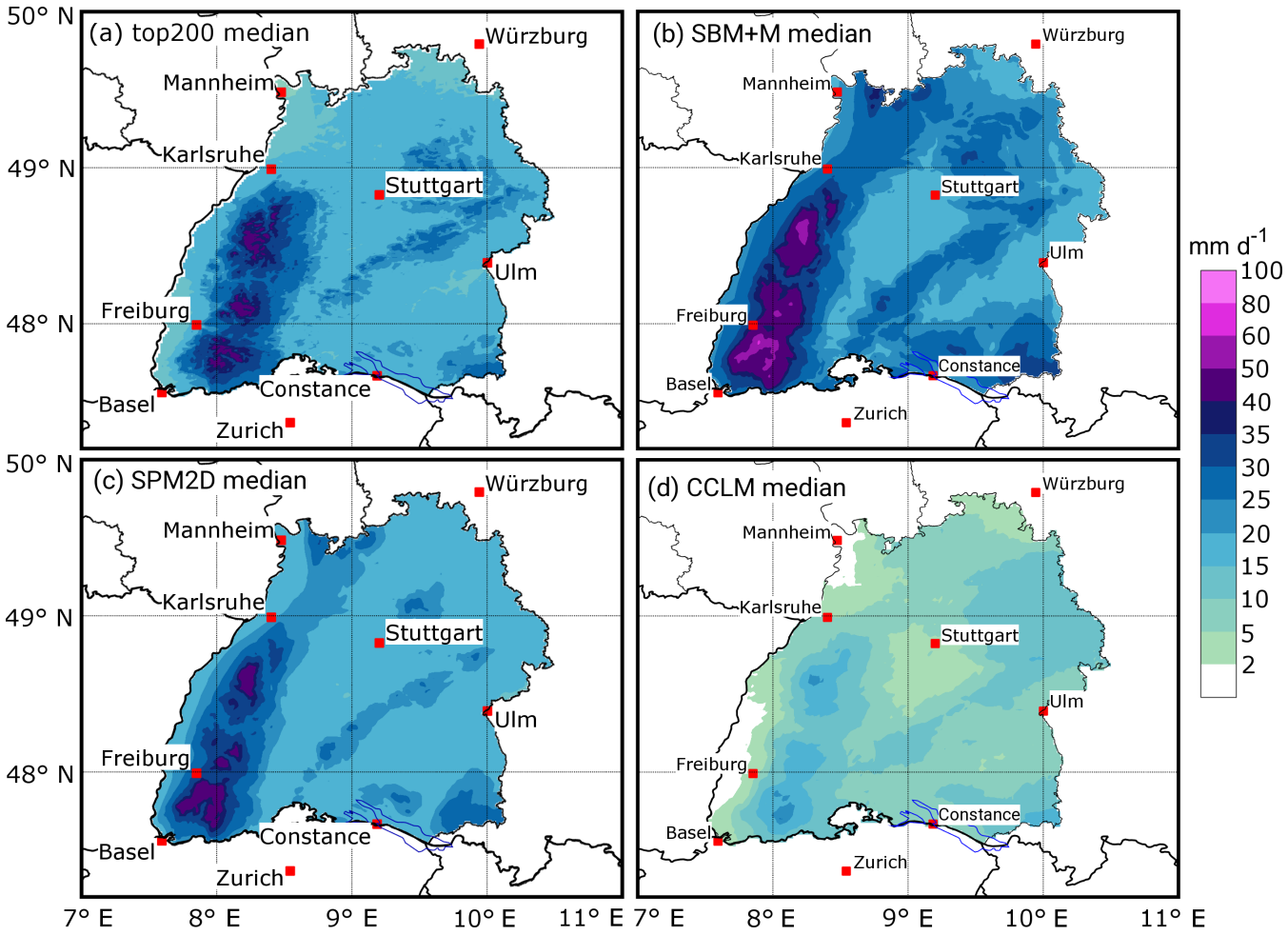


**Figure 12.** Precipitation fields for the median of (a) the top200 (REGNIE) events, (b) the SBM+M part of the stochastic events, (c) the full SPM2D stochastic event set , and (d) the CCLM simulations of the top REGNIE events.

Both ~~median and~~ the median and the 90th-percentile (p90) precipitation fields of the top200 ~~events and the SPM10k~~ event set and the SPM2D agree well concerning the spatial distribution ~~as well as~~ and the precipitation amounts (Figs. 12 and 13). Significant orographic ~~structures in the precipitation fields~~ precipitation enhancement over the Black Forest and Swabian Jura are clearly visible in all data sets. Note that the more detailed structure of the REGNIE data results from the regionalization method and its strong dependency on orography~~and~~ , which should not be over-interpreted. Larger spatial differences between the different realizations mainly appear in the ~~northern parts of Baden-Württemberg (the~~ Northern Rhine Valley and ~~northeastern rolling hills)~~ to the northeast of the domain for both the median and the p90~~field, whereat~~ , whereas for the latter, some differences also arise ~~in an additional area~~ northeast and southwest of Stuttgart. Nevertheless, all differences are small in the order of a few percent. The ~~rSPM~~ SBM+M shows an overestimation of precipitation ~~especially~~ over mountainous terrain,

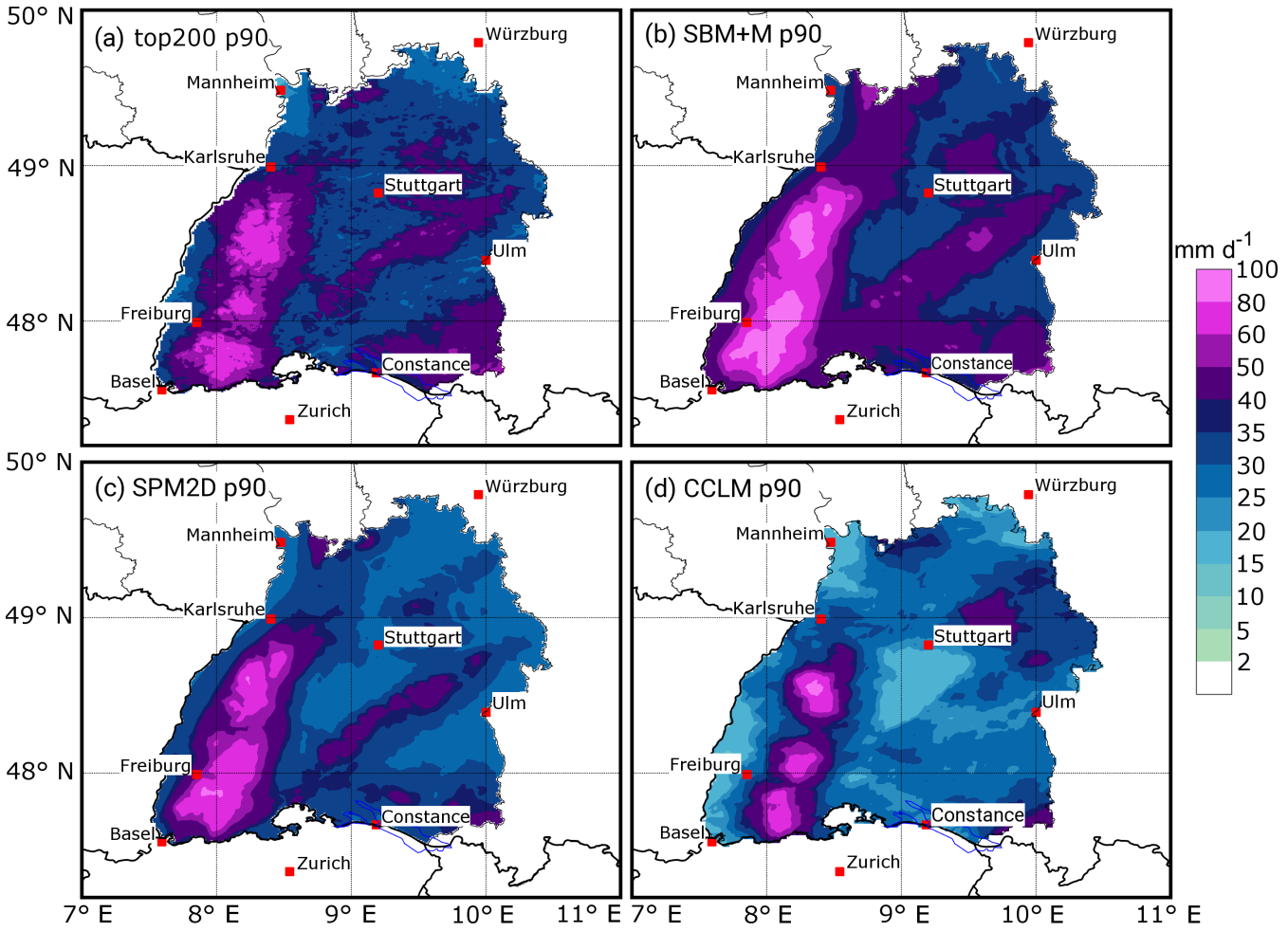


**Figure 13.** Precipitation fields for the ~~median~~ 90th percentile (p90) of (a) the top200 (REGNIE) events, (b) the ~~rSPM10k~~SBM+M part of the stochastic events, (c) the ~~SPM10k~~ full SPM2D stochastic event set, and (d) the CCLM simulations of the top REGNIE events.

~~whereas~~ while the CCLM simulates ~~overall less precipitation~~ less precipitation overall for the median. For the p90~~field~~, major differences appear especially ~~in low lands.~~ over the rolling terrain.

The areal rainfall of the ~~SPM10k median field~~ SPM2D median (Fig. 12) differs only about 3.3 % from the REGNIE top200, whereas that of the ~~rSPM10k~~ SBM+M is about 22.1 % higher. The spatial mean ~~precipitation~~ of the CCLM reanalysis is ~~barely~~ around half of REGNIE, which might be a result of the reduced sample size. The maximum values at any grid point ~~for~~ of the median field are about 7 % higher in the ~~SPM10k compared to~~ SPM2D compared to the REGNIE top200, and about 34 % higher in the ~~rSPM10k~~SBM+M realization, whereas the CCLM maximum ~~ist~~ is about 44 % smaller.

The areal rainfall for the p90 field (Fig. 13) is about 6.5 % smaller in ~~SPM10k~~SPM2D, and about 14 % higher in ~~rSPM10k~~ SBM+M, but about 22 % smaller in CCLM. The maximum values at any grid point ~~for~~ of the p90 field is approximately 1 %

smaller in ~~SPM10k~~SPM2D, and about 22 % higher in ~~rSPM10k~~ SBM+M and 13 % higher in CCLM. ~~Precipitation fields for the 90th percentile (p90) of (a) the top200 (REGNIE) events, (b) the rSPM10k, (c) the SPM10k, and (d) the CCLM simulations.~~

~~Comparing precipitation amounts for other percentiles , for example, between the 16th and 99th percentiles (Fig. ?? a), the~~ For other percentiles the differences between REGNIE and the SPM2D are very small for both the spatial mean ~~values~~ and the maximum precipitation at any grid point in the model domain ~~.~~ (Fig. S3 a). The differences become considerable only ~~for~~ above the 95th percentile~~and above~~. The SPM2D tends to overestimate lower precipitation amounts because the minimum values at any grid point are higher in the model than in the observations and invert for the 99th percentile only. In contrast, the differences between the ~~rSPM~~ SBM+M and REGNIE are considerably larger for maxima, minima and spatial means throughout every percentile. The CCLM reanalysis has a negative deviation for minimum and spatial mean precipitation ~~in~~ at all percentiles, whereas for the maximum values there is a marked underestimation for lower percentiles and an overestimation at higher percentiles.

At small percentiles, ~~or for small precipitation amounts, respectively,~~ the QIs, such as ~~correlation coefficient $r$, skill score~~ $r_{\mathrm{Sp}}$, $S$, ~~and normalized standard deviation~~ or $\hat{\sigma}_{\mathrm{f}}$, have low values due to the overestimation of the SPM2D (Fig. ??S3 b). The highest skill is reached around the 90th percentile with a slight decrease for higher values, which can be the result of the increasing uncertainties of the observations. Nevertheless, a skill score of around or above 0.8 confirms the reliability of the ~~simulations. Note that the QIs describe the performance of the SPM2D compared to REGNIE solely. In the following we concentrate our analysis on SPM2D and REGNIE. Comparison of (a) the maximum (red), the minimum (black), and the spatial mean precipitation (blue) of REGNIE (solid line), the SPM2D (dotted line), the rSPM (dashed line) and CCLM simulations (dot-dashed line), and (b) quality indices (QI) $r$, $S$, and $\hat{\sigma}_{\mathrm{f}}$ for different percentiles of the SPM2D compared to REGNIE.~~ stochastic simulations.

To estimate precipitation distributions for specific return periods, we fit a Gumbel ~~distribution (Wilks, 2006)~~ pdf to the annual maximum series of both REGNIE and ~~the SPM10k~~SPM2D. As it is not possible to directly estimate the time period and a corresponding annual maximum series for the stochastic event set, we count the number of stochastic values exceeding the 99th percentile of observations $n_{\mathrm{p99}}$ and normalize it by the probability of occurrence $p_{99}$, ~~giving~~ yielding the new time period~~$T_{\mathrm{SPM}}$~~:

$$T_{\mathrm{SPM}} = \frac{n_{\mathrm{p99}}}{p_{99}}\,. \tag{9}$$

After sorting the ~~SPM10k~~ SPM2D realizations in descending order, we take the first $n_T = T_{\mathrm{SPM}}$ values as the annual series of the ~~SPM10k~~ SPM2D and estimate a new Gumbel distribution. Using these distributions, we obtain precipitation values for specific return periods for both ~~the observations and the SPM10k~~REGNIE and SPM2D. This method is applied to both the spatial mean values of different areas and for every single grid point.

For a 10-year return period, the ~~SPM10k~~ SPM2D shows only small ~~deviations from~~ differences to REGNIE of less than $\pm$ 10 % over almost the entire area~~of Baden-Württemberg, with a small area of overestimation in the Southern Black Forest~~ ; only in a small region in the southern Black Forest precipitation is higher (Fig. 14 a). The areal mean difference is only 0.6 %. In the case of $T = 200$ ~~yrs~~ years (Fig. 14 b), the slight overestimation in the ~~Southern Black Forest remains with~~ southern Black

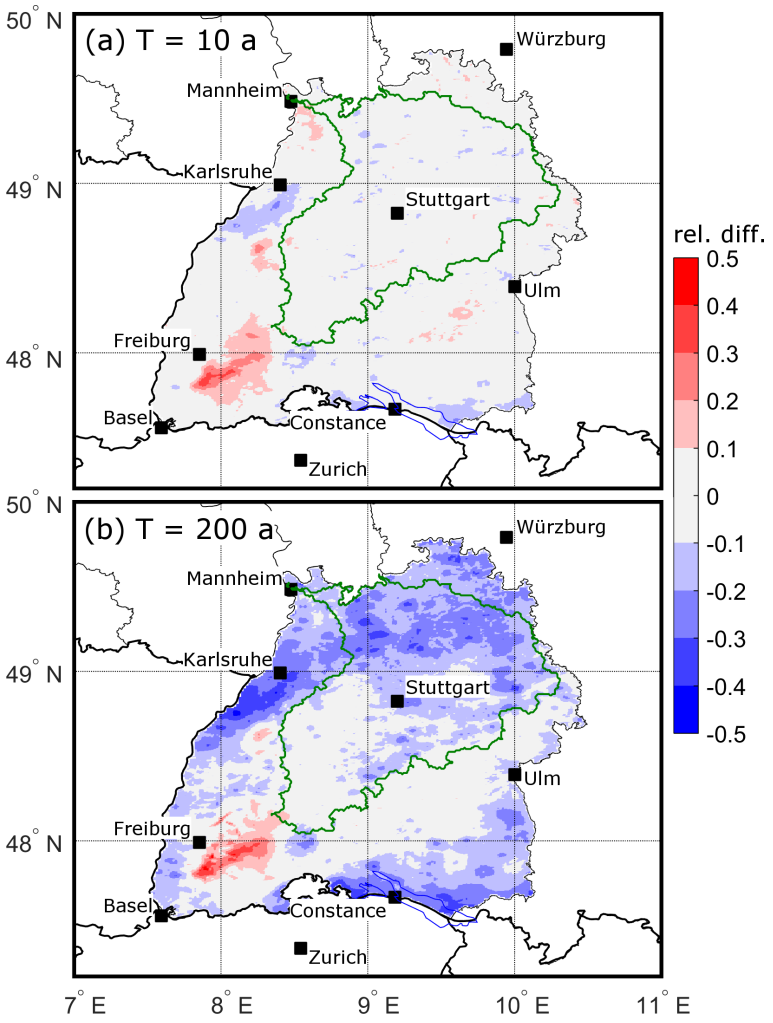


**Figure 14.** Relative difference of the precipitation amounts for return periods of (a) ~~a return period of~~ $T = 10$ years, and (b) $T = 200$ years, according to a Gumbel distribution fitted to the observations (top200) and the ~~SPM10k~~ SPM2D (see text for further explanation). The Neckar catchment is shown as green contour.

Forest area remains almost the same~~relative discrepancy~~. For this return period, the ~~SPM10k~~ SPM2D tends to underestimate precipitation, especially in the northern part of ~~Baden-Württemberg~~ BW and in the southeast around Lake Constance. Nevertheless, the ~~deviations~~ differences for most of the grid points are between $\pm 20\,\%$~~, and the~~ ; areal mean difference is about $-10\,\%$. Taking into account the ~~strongly increasing uncertainties of the observed values~~ increasing statistical uncertainty for higher return periods, ~~especially for $T > 100$ years,~~ this is still a reasonable result.

On the level of the major river catchments, the differences are small, too. For the Neckar catchment, for example (~~see~~ Fig. 14), which covers about 38 % of ~~Baden-Württemberg~~BW, the spatial mean deviation is about –0.5 % ~~in the case of~~ for

$T = 10$ ~~yrs~~ years and –12.7 % for the 200-year return period. Even for ~~the~~ catchments containing the area of overestimation in the Southern Black Forest~~(Upper Rhine between Basel and Mannheim, and High Rhine between Constance and Basel),~~ , the spatial mean deviations are between +1 and +4 % for $T = 10$ ~~yrs~~ years and between –2 and –10 % for $T = 200$ ~~yrs~~ years respectively.

Single grid point deviations and the ensuing spatial mean values as described above are sensitive to local conditions and uncertainties in both REGNIE and ~~SPM10k data~~SPM2D. Hence, we evaluate the model in a similar way by calculating ~~the~~ spatial mean precipitation first and then ~~fitting a Gumbel distribution to the spatial means in a second step. For the plotting, return period $T_k$ of each element $x_k$ of the annual maximum series with length $T_{max}$ is given by $T_k = T_{max} \cdot \mathrm{rk}^{-1}(x_k)$ with the rank $\mathrm{rk}(x_k)$ of element $x_k$ (annual series sorted in descending order). The first element (highest value) of an annual series of, for example, 100 years therefore has a return period of $T_1 = 100$ yrs, the second $T_2 = 50$ yrs, and so on. The values of $T_k$ were adjusted using the plotting position method of Cunnane (1978).~~

estimate the corresponding return periods (see Appendix A3). Again, the difference between ~~the simulated and observed spatial mean values of daily precipitation for the whole of Baden-Württemberg is small~~ SPM2D and REGNIE is small for entire BW, with slightly lower values from the simulations (Fig. 15 a). The distribution of the ~~SPM10k~~ SPM2D is very close and almost parallel to the estimated observed Gumbel distribution and within the 95 % confidence interval (CI95) estimated with the formula of Maity (2018). Considerable differences between the ~~SPM10k~~ SPM2D and REGNIE arise only for return periods of ~~$T = 1000$~~$T = 1{,}000$ ~~yrs and above~~years and above, but are still small. For the Neckar catchment, the ~~simulation results agree~~ SPM2D agrees well with the observed distribution for return periods up to ~~approximately 300~~ $T = 300$ years (Fig. 15 b). For higher return periods, the differences increase, but are still inside the CI95. Similar results can be found for other river catchments ~~. Note again that for such high return values, the statistical uncertainty of the observed distribution also increases significantly.~~ (not shown).

## 7 Summary and Conclusions

We have presented a novel method for estimating the statistics of ~~total~~ heavy rainfall based on a stochastic model approach ~~(SPM2D)~~. Total precipitation ~~at each grid point~~ is calculated from the linear superposition of four different parts: orographic precipitation, synoptic background precipitation, frontal precipitation and precipitation from convection embedded into mainly stratiform clouds. The linear theory of orographic precipitation according to Smith and Barstad (2004), which represents the core of the SPM2D, has been modified using three different calibration parameters to minimize the weaknesses found in previous studies such as the overestimation of wave dynamics and, thus, resulting precipitation and evaporation (e. g., Barstad and Smith, 2005; Kunz, 2011). For cross-validation, we calibrated and adjusted the SPM2D to a historic event set of heavy rainfall events (top200; training data). By adjusting appropriate ~~probability density functions (pdfs )~~ pdfs for all required model parameters, we simulated 10,000 independent stochastic precipitation events (validation data). The results were compared with observations and reanalysis data using different percentiles and return periods.

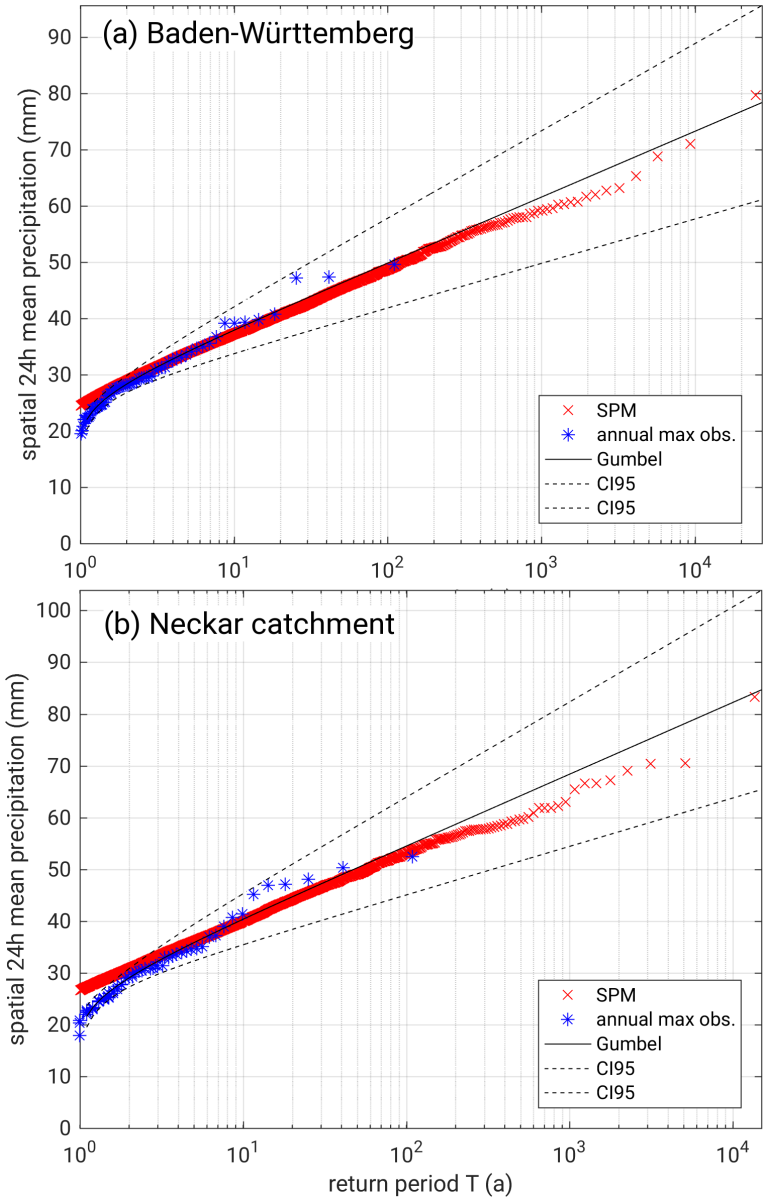


**Figure 15.** Daily rainfall totals (areal ~~mean~~means) as a function of return period $T$ based on the annual maximum series of observations (REGNIE, blue), the corresponding Gumbel distribution including the 95 % confidence intervals (black), and the annual ~~SPM10k~~ SPM2D series (red) for (a) the Federal State of Baden-Württemberg, and (b) the Neckar catchment.

The focus of the presented investigations was on the Federal State of Baden-Württemberg in Southwest Germany with the striking low-mountain ranges of Black Forest and Swabian Jura. The following main conclusions can be drawn:

- The SPM2D has a high skill to simulate both historic and stochastic heavy rainfall events. The simulated ~~spatial distributions~~ precipitation fields and magnitudes are reliable despite the simplified approach of the model initialized by a set of atmospheric variables obtained from radiosoundings. The differences between the SPM2D and REGNIE are small with deviations of less than 10 %. Local differences, however, may also ~~be traced back to uncertainties in REGNIEobservations~~result from the regionalization procedure of REGNIE, mainly because of ~~prevailing inhomogeneities in the spatial distribution~~ the low density of rain gauges ~~, especially~~ over mountainous terrain.

- The comparison of the SPM2D with the ~~reduced stochastic model rSPM~~ underlying linear approach of Smith and Barstad (2004) demonstrates the need ~~to additionally consider precipitation~~ for adjustments to the orographic precipitation formulation and for additionally precipitation parts related to frontal systems and embedded convection. The SPM2D with simplified parameterizations for these parts even yields more reliable precipitation fields for a historic event set compared to the sophisticated high-resolution NWP model CCLM.

- The solution of the model equations in Fourier space by an FFT allows for the simulation of a large number of events and to ~~run~~ operate the model in stochastic mode. Otherwise, the FFT restricts the model domain to a symmetric equidistant and mesoscale extent.

- The extent of the model domain, furthermore, has to be limited to ensure the validity of the assumption of spatially homogeneous distributed atmospheric conditions and synoptic forcing. This allows, for instance, for the usage of a ~~vertical profile from a single radiosounding station (or model data)~~single vertical profile.

- The presented stochastic approach is easily applicable to other investigation areas. Atmospheric variables for the initialization of the model can be estimated either from radiosoundings as within this study or using reanalysis or data from NWP models. Therefore, it can be applied to any region of the world with similar precipitation characteristics even if there is only a limited number of ground-based observations available.

As shown in our study, the SPM2D is sensitive to perturbations of ambient conditions. Therefore, high-quality input data, especially of the atmospheric parameters, are essential. On the other hand, the sensitivities of precipitation and rmse to changing input parameters is limited in a range of around ~~±10~~± 10 % of the original values, which is usually within the range of uncertainty. Using data of only one sounding station turned out to be sufficient to achieve reliable heavy rainfall fields. As shown by (Kunz, 2011), the differences to another upstream sounding station (Nancy in France) are small, at least in the mean. This, however, applies only for widespread precipitation with ~~durations~~ duration over several hours to days, which is also the focus of our study. Intermittent or even mainly convectively-driven events cannot be reliably reproduced by our model.

The input parameters can be considered as independent, as just a few cases revealed higher ~~correlation~~correlations. The sensitivity of the model for these parameters, however, turned out to be week. Additionally, the correlation coefficients between the model input parameters vary among the seasons.

To transfer the method to another investigation area and future risk assessments, just a few steps are necessary: first a proper sample of historical heavy rainfall events. In the next step, the statistics (pdfs) of the prevailing ambient conditions, background

precipitation, and duration for the event set have to be calculated. Finally, the ~~reduced SPM (rSPM)~~ non-stochastic part of the SPM2D has to be calibrated by determining appropriate values for the free model tuning parameters.

The ~~presented~~ output of SPM2D is a certain number of independent heavy precipitation events and not a continuous time series. We have presented a method to convert this to a equivalent time period, which is mostly necessary for risk assessments, by counting the number of days in SPM2D above a defined threshold and normalizing it by the corresponding probability of the observations. Using this total time span it is possible to estimate the return period of every single event and a corresponding new pdf. The time between two events is assumed as dry period.

The presented SPM2D is part of the project FLORIS (Flood Risk), which represents a novel risk assessment methodology for an entire domain and not only for single catchments ~~applied~~ usually considered in the insurance industry. Within the framework of this project, the SPM2D was applied to other federal states in central Germany. The modeled precipitation fields are used as input data for hydrological and hydraulic simulations, from which the flood risk can be estimated, for example for a one-in-200-years event required according to the insurance regulation of Solvency II. However, the results of the SPM2D basically can be used for several different applications such as water management or the design of flood protection measures.

## 8 Data availability

The REGNIE data used in this paper are freely available for research and can be requested at the DWD (doi:10.1127/0941-2948/2013/0436); The sounding data are freely available from the Integrated Global Radiosonde Archive (https://www.ncdc.noaa.gov/data-access/weather-balloon/integrated-global-radiosonde-archive). The required orographic data can be obtained from http://srtm.csi.cgiar.org/ (doi:10.1080/13658810601169899).

## Appendix A: Statistical quantities

### A1 Probability Density Functions

We used the 20 probability density functions (pdfs) preset in the MATLAB statistical toolbox (MATLAB, 2016) plus the circular von-Mises distribution for wind speed (Mardia and Zemroch, 1975). In total, 17 pdfs were suitable and tested and compared with the observed distribution of each parameter for each of the four seasons (Table A1). Note that the Gumbel (GbD) and Weibull (WbD) distributions are special cases of the generalized extreme value distribution (GEV) and that some pdfs cannot be used due to their ranges.

### A2 Skill Score

In this study we use the skill score $S$ introduced by Taylor (2001):

$$S = \frac{4(1+r)}{\left(\hat{\sigma}_f + \frac{1}{\hat{\sigma}_f}\right)^2 \cdot (1+r_0)}, \tag{A1}$$

**Table A1.** List of the tested and suitable pdfs preset in the MATLAB statistical toolbox (the short acronyms in brackets are for further orientation).

| | |
|---|---|
| Birnbaum-Saunders (BSD) | Nakagami (NkD) |
| Gamma (GmD) | Normal (ND) |
| Generalized Extreme Value (GEV) | Poisson (PD) |
| Gumbel (GbD) | Rayleigh (RyD) |
| Half-Normal (HND) | Rician (RcD) |
| Inverse Gaussian (IGD) | Stable (SD) |
| Logistic (LD) | Student's t (StD) |
| Log-Logistic (LLD) | Weibull (WbD) |
| Log-Normal (LND) | |

where $r$ is the correlation coefficient after Spearman (1904) between modeled and observed precipitation field, $r_0$ is the maximum attainable correlation, and $\hat{\sigma}_f = \sigma_{\mathrm{mod}} \cdot \sigma_{\mathrm{obs}}^{-1}$ is the normalized standard deviation with the standard deviations of the model (SBM+M) $\sigma_{\mathrm{mod}}$ and observations (REGNIE) $\sigma_{\mathrm{obs}}$. For $\hat{\sigma}_f \to 1$ and for $r \to r_0$, $S$ approaches unity, which is the best result. Furthermore, Taylor (2001) provided no regulation for the estimation of $r_0$. Therefore, we set $r_0$ to the maximum calculated correlation coefficient of all simulations. As it is not guaranteed that this maximum is the actual maximum attainable correlation, we increase $r_0$ by 10 %, yielding $r_0 = 0.93$. According to Taylor (2001), the use of correlation and standard deviation is more stable compared to rmse or bias.

### A3 Return Periods

For the estimation of return periods, the annual maximum series with length $T_{max}$ of the data set is sorted in descending order. Then, the return period $T_k$ of each element $x_k$ of this series is given by $T_k = T_{max} \cdot \mathrm{rk}^{-1}(x_k)$ with the rank $\mathrm{rk}(x_k)$ of element $x_k$. The first element (highest value) of the annual series of, for example, $T_{max} = 100$ yrs, has a return period of $T_1 = 100$ yrs, the second of $T_2 = 50$ yrs, and so on. For the visualization, the values of $T_k$ were adjusted using the plotting position method of Cunnane (1978).

*Competing interests.* The authors declare that they have no conflict of interest.

*Acknowledgements.* The authors thank a local insurance company for funding the project. We also would like to thank the German Weather Service (DWD) and the Integrated Global Radiosonde Archive (IGRA) for providing different observational data sets and CGIAR-CSI for the orographic data. Special thanks go to James Daniell, Andreas Kron and Simon Hoellering from ~~KIT~~ the Karlsruhe Institute of Technology

(KIT) for constructive discussions ~~within~~ during the project and for valuable suggestions ~~during~~ of the model development. We acknowledge support by Deutsche Forschungsgemeinschaft (DFG) and open access publishing fund of ~~Karlsruhe Institute of Technology (KIT)~~KIT. We are grateful to the constructive comments and suggestions of ~~three anonymous~~ the reviewers that helped to improve the quality of this paper.

## References


Barstad, I. and Caroletti, G. N.: Orographic precipitation across an island in southern Norway: model evaluation of time-step precipitation, Q. J. R. Meteorol. Soc., 139, 1555–1565, 2013.

Barstad, I. and Smith, R. B.: Evaluation of an Orographic Precipitation Model, J. Hydrometeorol., 6, 85–99, 2005.

Basist, A., Bell, G. D., and Meentmeyer, V.: Statistical relationships between topography and precipitation patterns, J. Climate, 7, 1305–1315, 1994.

Bergeron, T.: On the physics of fronts, Bull. Am. Meteorol. Soc., 18, 265–275, 1937.

Browning, K. A., Pardoe, C. W., and Hill, F. F.: The nature of orographic rain at wintertime cold fronts, Q. J. R. Meteorol. Soc., 101, 333–352, 1975.

Cannon, D. J., Kirshbaum, D. J., and Gray, S. L.: Under what conditions does embedded convection enhance orographic precipitation?, Q. J. R. Meteorol. Soc., 138, 391–406, 2012.

Caroletti, G. N. and Barstad, I.: An assessment of future extreme precipitation in western Norway using a linear model, Hydrol. Earth Syst. Sci., 14, 2329–2341, 2010.

Crochet, P., Jóhannesson, T., Jónsson, T., Sigurdsson, O., Björnsson, H., Pálsson, F., and Barstad, I.: Estimating the spatial distribution of precipitation in Iceland using a linear model of orographic precipitation, J. Hydrometeorol., 8, 1285–1306, 2007.

Cross, D., Onof, C., Winter, H., and Bernardara, P.: Censored rainfall modelling for estimation of fine-scale extremes, Hydrol. Earth Syst. Sci. Discuss., https://doi.org/10.5194/hess-2017-437, 2017.

Cunnane, C.: Unbiased plotting positions – a review, J. Hydrol., 37, 205–222, 1978.

Drogue, G., Humbert, J., Deraisme, J., Mahr, N., and Freslon, N.: A statistical-topographic model using an omnidirectional parameterization of the relief for mapping orographic rainfall, Int. J. Climatol., 22, 599–613, https://doi.org/10.1002/joc.671, 2002.

Duckstein, L., Bárdossy, A., and Bogárdi, I.: Linkage between the occurrence of daily atmospheric circulation patterns and floods: an Arizona case study, J. Hydrol., 143, 413–428, 1993.

Durran, D. R. and Klemp, J. B.: On the effects of moisture on the Brunt-Väisälä frequency, J. Atmos. Sci., 39, 2152–2158, 1982.

Durre, I., Vose, R. S., and Wuertz, D. B.: Overview of the integrated global radiosonde archive, J. Climate, 1151, 53–68, 2006.

Eliassen, A.: On the vertical circulation in frontal zones, Geophys. Publ., 24, 147–160, 1962.

Fluck, E.: Hail statistics for European countries, Phd thesis, Institute of Meteorology and Climate Research (IMK), Karlsruhe Institute of Technologie (KIT), Karlsruhe, Germany, https://doi.org/10.5445/IR/1000080663, 2018.

Freedman, D. and Diaconis, P.: On the histogram as a density estimator: L2 theory, Zeitschrift für Wahrscheinlichkeitstheorie und Verwandte Gebiete, 57, 453–476, https://doi.org/10.1007/BF01025868, 1981.

Fuhrer, O. and Schär, C.: Embedded cellular convection in moist flow past topography, J. Atmos. Sci., 62, 2810–2828, 2005.

Furrer, E. M. and Katz, R. W.: Generalized linear modeling approach to stoachstic weather generators, Clim. Res., 34, 129–144, 2007.

Goovaerts, P.: Geostatistical approaches for incorporating elevation into the spatial interpolation of rainfall, J. Hydrol., 228, 113–129, 2000.

Handwerker, J.: Cell tracking with TRACE3D - a new algorithm, Atmos. Res., 61, 15–34, 2002.

Houze, R. A. and Hobbs, P. V.: Organization and Structure of Precipitation cloud systems, Adv. Geophys., 24, 225–315, 1982.

Jiang, Q. and Smith, R. B.: Cloud timescales and orographic precipitation, J. Atmos. Sci., 60, 1543–1559, 2003.

Kållberg, P., Simmons, A., Uppala, S., and Fuentes, M.: The ERA-40 archive. [Revised October 2007], Shinfield Park, Reading, 2004.

Kienzler, S., Pech, I., Kreibich, H., Müller, M., and Thieken, A. H.: After the extreme flood in 2002: changes in preparedness, response and recovery of flood-affected residents in Germany between 2005 and 2011, Nat. Hazards Earth Syst. Sci., 15, 505–526, 2015.

Kirshbaum, D. J. and Durran, D. R.: Factors governing cellular convection in orographic precipitation, J. Atmos. Sci., 61, 682–698, 2004.

Kirshbaum, D. J. and Smith, R. B.: Temperature and moist-stability effects on midlatitude orographic precipitation, Q. J. R. Meteorol. Soc., 134, 1183–1199, https://doi.org/10.1002/qj.274, 2008.

Koutsoyiannis, D., Kozonis, D., and Manetas, A.: A mathematical framework for studying rainfall intensity-duration-frequency relationships, J. Hydrol., 206, 118–135, 1998.

Kunz, M.: Characterisitics of Large-Scale Orographic Precipitation in a Linear Perspective, J. Hydrometeorol., 12, 27–44, 2011.

Kunz, M. and Wassermann, S.: Moist dynamics and sensitivity of orographic precipitation to changing ambient conditions in an idealised perspective, Meteorol. Z., 20, 199–215, 2011.

Lalas, D. P. and Einaudi, F.: On the stability of a moist atmosphere in the presence of a background wind, J. Atmos. Sci., 30, 795–800, 1973.

Laube, N.: personal correspondence, Phd thesis, Institute of Meteorology and Climate Research (IMK), Karlsruhe Institute of Technologie (KIT), Karlsruhe, Germany, 2018.

Maity, R.: Statistical Methods in Hydrology and Hydroclimatology, Springer Nature Singapore Pte Ltd., https://doi.org/10.1007/978-981-10-8779-0, 2018.

Mardia, K. V. and Zemroch, P. J.: Algorithm AS 86: The Von Mises Distribution Function, Journal of the Royal Statistical Society. Series C (Applied Statistics), 24, 268–272, 1975.

Marra, F., Morin, E., Peleg, N., Mei, Y., and Anagnostou, E. N.: Intensity–duration–frequency curves from remote sensing rainfall estimates: comparing satellite and weather radar over the eastern Mediterranean, Hydrol. Earth Syst. Sci., 21, 2389–2404, https://doi.org/10.5194/hess-21-2389-2017, 2017.

Mason, B.: The physics of clouds, Oxford University Press, 671 pp., 1971.

MATLAB: MATLAB and Statistics Toolbox Release 2016b, (version 9.1), The MathWork Inc., Natick, Massachusetts, USA, http://de.mathworks.com/help/, last visited 10 August 2017, 2016.

Mohr, S. and Kunz, M.: Recent trends and variabilities of convective parameters relevant for hail events in Germany and Europe, Atmos. Res., 123, 211–228, 2013.

MunichRe: NatCatSERVICE, natcatservice.munichre.com/, accessed: 28 Sept 2017, 2017.

Neykov, N. M., Neytchev, P. N., and Zucchini, W.: Stochstic daily precipitation model with a heavy-tailed component, Nat. Hazards Earth Syst. Sci., 14, 2321–2335, https://doi.org/10.5194/nhess-14-2321-2014, 2014.

Palutikov, J. P., Brabson, B., Lister, D. H., and Adcock, S. T.: A review of methods to calculate extreme wind speeds, Meteorol. Appl., 6, 119–132, 1999.

Peleg, N., Marra, F., Fatichi, S., Paschalis, A., Molnar, P., and Burlando, P.: Spatial variability of extreme rainfall at radar subpixel scale, J. Hydrol., 556, 922 – 933, https://doi.org/10.1016/j.jhydrol.2016.05.033, 2018.

Petrow, T., Zimmer, J., and Merz, B.: Changes in the flood hazard in Germany through changing frequency and persistence of circulation patterns, Nat. Hazards Earth Syst. Sci., 9, 1409, 2009.

Piper, D., Kunz, M., Ehmele, F., Mohr, S., Mühr, B., Kron, A., and Daniell, J.: Exceptional sequence of severe thunderstorms and related flash floods in May and June 2016 in Germany-Part 1: Meteorological background, Nat. Hazards Earth Syst. Sci., 16, 2835, 2016.

Rauthe, M., Steiner, H., Riediger, U., A., M., and Gratzki, A.: A Central European precipitation climatology - Part I: Generation and validation of a high-resolution gridded daily data set (HYRAS), Meteorol. Z., 22, 235–256, 2013.

Richardson, C. W.: Stochastic Simulation of Daily Precipitation, Temperature, and Solar Radiation, Water Resour. Res., 17, 182–190, 1981.

Rockel, B., Will, A., and Hense, A.: The regional climate model COSMO-CLM (CCLM), Meteorol. Z., 17, 347–348, 2008.

Schröter, K., Kunz, M., Elmer, F., Mühr, B., and Merz, B.: What made the June 2013 flood in Germany an exceptional event? A hydro-meteorological evaluation, Hydrol. Earth Syst. Sci., 19, 309–327, 2015.

Smith, R. B.: Linear theory of stratified hydrostatic flow past an isolated mountain, Tellus, 32, 348–364, 1980.

Smith, R. B.: Hydrostatic airflow over mountains, Adv. Geophys., 31, 1–41, 1989.

Smith, R. B. and Barstad, I.: A Linear Theory of Orographic Precipitation, J. Atmos. Sci., 61, 1377–1391, 2004.

Spearman, C.: The Proof and Measurement of Association between Two Things, The American Journal of Psychology, 15, 72–101, 1904.

Taylor, K. E.: Summarizing multiple aspects of model performance in a single diagram, J. Geophys. Res., 106, 7183–7192, 2001.

Uhlemann, S., Thieken, A. H., and Merz, B.: A consistent set of trans-basin floods in Germany between 1952-2002, Hydrol. Earth Syst. Sci., 14, 1277, 2010.

Wanner, H., Rickli, R., Salvisberg, E., Schmutz, C., and Schüepp, M.: Global climate change and variability and its influence on alpine climate-concepts and observations, Theor. Appl. Climatol., 58, 221–243, 1997.

Wilks, D. S.: Statistical Methods in the Atmospheric Sciences, vol. 91 of *International Geophysics Series*, Academie Press, San Diego, California, USA, 2nd edn., 2006.